

CERN-EP-2018-254
2019/04/09

CMS-B2G-17-017

Search for resonant $t\bar{t}$ production in proton-proton collisions at $\sqrt{s} = 13$ TeV

The CMS Collaboration*

Abstract

A search for a heavy resonance decaying into a top quark and antiquark ($t\bar{t}$) pair is performed using proton-proton collisions at $\sqrt{s} = 13$ TeV. The search uses the data set collected with the CMS detector in 2016, which corresponds to an integrated luminosity of 35.9 fb^{-1} . The analysis considers three exclusive final states and uses reconstruction techniques that are optimized for top quarks with high Lorentz boosts, which requires the use of nonisolated leptons and jet substructure techniques. No significant excess of events relative to the expected yield from standard model processes is observed. Upper limits on the production cross section of heavy resonances decaying to a $t\bar{t}$ pair are calculated. Limits are derived for a leptophobic topcolor Z' resonance with widths of 1, 10, and 30%, relative to the mass of the resonance, and exclude masses up to 3.80, 5.25, and 6.65 TeV, respectively. Kaluza–Klein excitations of the gluon in the Randall–Sundrum model are excluded up to 4.55 TeV. To date, these are the most stringent limits on $t\bar{t}$ resonances.

Published in the Journal of High Energy Physics as doi:10.1007/JHEP04(2019)031.

arXiv:1810.05905v2 [hep-ex] 6 Apr 2019

1 Introduction

The top quark (t) is the most massive known fundamental particle [1, 2] in the standard model. It has a Yukawa coupling to the Higgs field that is near unity. It is also closely connected to the hierarchy problem, where the largest corrections to the Higgs mass arise from top quark loops. Furthermore, studies of the top quark may provide insight into the mechanism of electroweak (EW) symmetry breaking.

Many theories beyond the standard model (SM) predict heavy resonances at the TeV scale, which would decay to top quark and antiquark ($t\bar{t}$) pairs. These resonances can present themselves as peaks on top of the falling $t\bar{t}$ invariant mass spectrum or as a distortion of the $t\bar{t}$ spectrum if the resonance has a large width and a mass above the center-of-mass energy of the colliding partons. Resonances decaying to $t\bar{t}$ pairs can be found in models that contain TeV scale color singlet Z' bosons [3–5], a pseudoscalar Higgs boson that may couple strongly to $t\bar{t}$ pairs [6], axigluons [7–9], or colorons [10–13], and especially models that contain a leptophobic topcolor Z' [14]. Additionally, extensions of the Randall–Sundrum model [15, 16] with extra dimensions predict Kaluza–Klein (KK) excitations of the gluons g_{KK} [17] or gravitons G_{KK} [18], which can have large branching fractions to $t\bar{t}$ pairs. This analysis searches for spin-1 resonances that do not interfere with SM $t\bar{t}$ production. Previous searches at the Fermilab Tevatron have excluded a leptophobic Z' boson up to 900 GeV [19–24] at 95% confidence level (CL). Experiments at the CERN LHC have excluded various Z' and g_{KK} models at 95% CL in the 1–4 TeV mass range [25–32]. The results presented here represent a significant improvement on the previous searches for $t\bar{t}$ resonances.

This paper presents a model-independent search for $t\bar{t}$ resonances. Since no excess is seen, limits are calculated on several spin-1 resonance models of varying widths. The $t\bar{t}$ system, and all its daughter particles, decay as described by the SM. The top quark predominately decays to a W boson and a bottom quark (b). Each of the two W bosons in the event can decay to either a lepton and its corresponding neutrino or to hadrons. The analysis considers three subanalyses based on the decay modes of the two W bosons: dilepton, single-lepton, and fully hadronic decay modes of the $t\bar{t}$ system. In the fully hadronic channel, both W bosons decay to hadrons. In the single-lepton channel, one W boson decays to an electron (e) or muon (μ) and its neutrino (ν) counterpart, while the other W boson decays to hadrons. In the dilepton channel, both W bosons decay to an e or μ and a ν . The leptonic selections are not optimized to identify electrons or muons originating from leptonically decaying tau leptons; however, such particles are not excluded by the event selections. The search is based on $\sqrt{s} = 13$ TeV proton-proton (pp) collision data collected in 2016 by the CMS experiment at the LHC, corresponding to an integrated luminosity of 35.9 fb^{-1} .

The dilepton final state consists of two leptons ($\mu\mu$, ee , or μe), two jets originating from bottom quarks (b jets) with high transverse momentum (p_T), and missing transverse momentum (\vec{p}_T^{miss}). The large mass of the resonance causes the resulting top quarks to have a significant Lorentz boost, which leads to a collimated system consisting of a lepton and a b jet. To account for the overlap between the lepton and the b jet, special reconstruction and selection criteria are used to increase lepton selection efficiency and reduce the SM background. The dominant irreducible SM background arises from $t\bar{t}$ nonresonant production. Smaller contributions are due to a Z boson produced in association with jets (Z +jets), single top quark, and diboson processes. Events that have a large separation between the lepton and b jet are allocated to control regions (CR), which are used to validate the modeling of the SM backgrounds.

The single-lepton final state consists of one lepton (μ or e), at least two high- p_T jets, and \vec{p}_T^{miss} . In this channel also, the final state particles from the decay of the $t\bar{t}$ pairs have a large Lorentz

boost because of the mass of the resonance. Leptons from the decay of the W boson are found in near proximity to the b jet from the top quark decay. The same lepton reconstruction and selection criteria used in the dilepton channel are used in the single-lepton channel. In addition to those techniques, a special triggering technique is used to select events with a single nonisolated lepton and an additional jet. A t tagging algorithm is used to identify top quarks where the daughter W boson decays hadronically ($t \rightarrow W b \rightarrow q\bar{q}'b$). Events with a jet that passes the t tagging criteria are classified into a category with higher sensitivity. The largest irreducible background is the $t\bar{t}$ continuum production, while the largest reducible background is from W bosons produced in association with jets (W+jets). The latter background is separated from the signal using a multivariate analysis technique.

The fully hadronic channel contains events with a dijet topology, where both large radius jets are required to pass t tagging criteria that select Lorentz-boosted hadronically decaying top quarks. Because of the dijet topology of the search region, the largest reducible background arises from dijet events produced from quantum chromodynamic (QCD) interactions between the colliding protons. This background, referred to as QCD multijet production, can be reduced considerably by requiring one of the subjects in each of the two large radius jets, which are selected by the t tagging algorithm, to be consistent with the fragmentation of a bottom quark [33]. A subjet is defined as a smaller radius jet reconstructed within a larger radius jet. The use of subjet b tagging for categorization nearly eliminates the QCD multijet background leaving only the $t\bar{t}$ continuum in the highest sensitivity category.

Except for the QCD multijet background in the fully hadronic channel, the shapes of all SM backgrounds are estimated from simulation. The total normalization of each simulated sample is obtained from a simultaneous binned maximum likelihood fit to the reconstructed $t\bar{t}$ invariant mass ($m_{t\bar{t}}$) distribution for the single-lepton and fully hadronic analyses and S_T for the dilepton analysis, where S_T is defined as

$$S_T = \sum_{i=1}^{N_{\text{jet}}} p_{T_i}^{\text{jet}} + \sum_{i=1}^2 p_{T_i}^{\ell} + p_T^{\text{miss}}. \quad (1)$$

The variable S_T is used because it has a greater sensitivity to signal than $m_{t\bar{t}}$, in the dilepton final state. A limit on the production cross section of heavy resonances is extracted by performing a template-based statistical evaluation of the $m_{t\bar{t}}$ (single-lepton and fully hadronic) and S_T (dilepton) distributions simultaneously in all of the channels.

This paper is organized the following way. Section 2 provides a description of the CMS detector. The reconstruction and identification of electrons, muons, and jets are described in Section 3. Section 3 also gives an overview of the t tagging algorithms used. The data sets and triggering techniques are described in Section 4. The simulated Monte Carlo (MC) samples used in the analysis are discussed in Section 5. Section 6 describes the event selection for the three different channels. Section 7 describes the evaluation of the SM background processes. Systematic uncertainties affecting the signal and background shapes and normalization are discussed in Section 8. The statistical analysis and the results are given in Sections 9 and 10, respectively, and a summary is presented in Section 11.

2 The CMS detector

The central feature of the CMS detector is a superconducting solenoid of 6 m internal diameter, providing a magnetic field of 3.8 T. Within the solenoid volume are a silicon pixel and strip tracker, a lead tungstate crystal electromagnetic calorimeter (ECAL), and a brass and scintillator

hadron calorimeter (HCAL), each composed of a barrel and two endcap sections. In addition to the barrel and endcap detectors, CMS has extensive forward calorimetry. Muons are detected by four layers of gas-ionization detectors embedded in the steel flux-return yoke of the magnet. The inner tracker measures charged-particle trajectories within the pseudorapidity range $|\eta| < 2.5$, and provides an impact parameter resolution of approximately $15 \mu\text{m}$. A two-stage trigger system [34] selects pp collision events of interest for use in physics analyses. A more detailed description of the CMS detector, together with a definition of the coordinate system used and the relevant kinematic variables, can be found in Ref. [35].

3 Event reconstruction

The CMS event reconstruction uses a particle-flow (PF) technique that aggregates input from all subdetectors for event reconstruction [36]. Typical examples of PF inputs are charged-particle tracks from the tracking system and energy deposits from the ECAL and HCAL. The PF approach enables the global event description to take advantage of the excellent granularity of the CMS detector. Clusters of tracks and energy deposits are iteratively classified as muons, electrons, photons, charged hadrons, and neutral hadrons. Vertices are reconstructed from tracks using a deterministic annealing filter algorithm [37]. The reconstructed vertex with the largest value of summed physics-object p_{T}^2 is taken as the primary pp interaction vertex (PV). For the PV reconstruction, the physics objects are jets, clustered with the jet finding algorithm [38, 39] using only tracking information, with the tracks assigned to the PV as inputs. The reconstructed leptons and photons in the event are included as inputs to the jet clustering algorithm.

The $\vec{p}_{\text{T}}^{\text{miss}}$ is defined as the projection onto the plane perpendicular to the beam axis of the negative vector sum of the momenta of all reconstructed PF candidates in an event [40]. Its magnitude is referred to as $p_{\text{T}}^{\text{miss}}$. Corrections to the jet energy scale and jet energy resolution are propagated to the measurement of $p_{\text{T}}^{\text{miss}}$.

Muons are reconstructed in the pseudorapidity range $|\eta| < 2.4$ using the information from the tracker and muon chambers [37]. Tracks associated with muon candidates must be consistent with a muon originating from the PV, and tracks must satisfy fit quality requirements.

Electrons are detected and measured in the pseudorapidity range $|\eta| < 2.5$, by combining tracking information with energy deposits in the ECAL [41, 42]. Candidate electrons are required to originate from the PV. The track quality, electromagnetic shower shape, displacement between the track and electromagnetic shower, and ratio of energy between the HCAL and ECAL are used to identify electrons. Reconstructed electrons that originate from photon conversions are rejected.

No isolation requirements are placed on the leptons at the trigger or analysis level. This is because the lepton, bottom quark, and neutrino from the top quark decay are highly collimated, and the lepton is not well separated from the products of fragmentation of the bottom quark. Additionally, jets that contain an electron are reclustered and corrected with the track and calorimeter deposit of the electron removed. Kinematic restrictions are placed on the electron and on the overall event to reduce the contribution from electrons not originating from t decays. Details on these requirements can be found in Section 6.

The PF candidates are clustered into jets using the FASTJET software package [39]. Charged hadrons that are not associated with the PV in the event are excluded from the jet clustering procedure via charged hadron subtraction (CHS) [36]. All jets are required to have $|\eta| < 2.4$.

Jets are clustered using the anti- k_T jet clustering algorithm [38] with a distance parameter of 0.4 (AK4 jets). If a lepton is found with $\Delta R < 0.4$ of an AK4 jet, its four-momentum is subtracted from that of the jet. The single-lepton and fully hadronic analyses also use anti- k_T clustered jets with a distance parameter of 0.8 (AK8 jets). These larger-radius jets are used to tag the hadronic decay of top quarks. A high-mass resonance decay creates daughter particles with significant Lorentz boost. The three jets from the top quark decay merge into a single-larger AK8 jet. Jets in all three channels are contaminated with neutral particles that are generated from additional pp collisions within the same or a neighboring bunch crossing (pileup). The extra energy in each jet is corrected based on the average expectation of the pileup within the jet footprint [43]. The expected energy offset due to pileup is modeled as a function of the number of primary vertices in the event [40]. Jets that are produced from the decay of charm and bottom quarks are identified using the combined secondary vertex algorithm (CSV) [44]. Loose, medium, and tight operating points are used in this analysis. They have a probability of 10, 1, and 0.1%, respectively, of misidentifying a light-parton jet as heavy flavor, where the light-flavor jet has $p_T > 30$ GeV and is determined from a simulated multijet sample with a center-of-mass energy between 80 and 120 GeV [33]. They correspond to a b tagging efficiency of 81, 63, and 41%, respectively, for b jets ($p_T > 20$ GeV) in simulated $t\bar{t}$ events. All jets are required to pass a minimal set of criteria to separate them from calorimeter noise and other sources of jets that do not originate from the PV [45]. Events are also required to pass a set of selections that remove spurious p_T^{miss} that is generated from calorimeter noise [46].

The t tagging algorithm [47, 48], which is based on the algorithm described in Ref. [49], is applied to AK8 jets that use pileup per particle identification (PUPPI) corrections [50], referred to as PUPPI jets, in order to separate hadronically decaying top quarks from light quark or gluon jets. While CHS only removes charged particles originating from pileup, PUPPI corrects for both charged and neutral pileup particles. PUPPI jets, as opposed to CHS jets, are therefore used for t tagging because of their better performance as a function of pileup. The CMS t tagging algorithm only considers jets with $p_T > 400$ GeV, as lower-momentum top quarks frequently decay into resolved jets. The algorithm iteratively reverses the jet clustering procedure in order to remove soft radiation. First, it reclusters the AK8 PUPPI jet with the Cambridge-Aachen jet clustering algorithm [51]. It then separates the jet (j) into two subjets, j_1 and j_2 , which must satisfy the “soft drop” (SD) criterion

$$\frac{\min(p_{T1}, p_{T2})}{p_{T1} + p_{T2}} > z_{\text{cut}} \left(\frac{\Delta R_{12}}{R_0} \right)^\beta, \quad (2)$$

where p_{T1} and p_{T2} are the transverse momenta of the two subjets and ΔR_{12} is the distance between them. The implementation of the SD algorithm used in this analysis has an angular exponent $\beta = 0$, making it equivalent to the “modified mass drop tagger” algorithm [52]. Additionally, a soft cutoff threshold of $z_{\text{cut}} = 0.1$ and a characteristic radius $R_0 = 0.8$ [53] are used. If the SD criterion is met, the procedure ends with j as the resulting jet. If not, the lower- p_T subjet is discarded and the declustering procedure continues with the higher- p_T subjet. The SD mass (m_{SD}) of the jet pair is required to be near the mass of the top quark ($105 < m_{\text{SD}} < 210$ GeV). The CMS t tagging algorithm also requires that the N -subjettiness [54, 55] ratio ($\tau_3 \equiv \tau_3/\tau_2$) must be less than 0.65. The N -subjettiness (τ_N) is a measure of the consistency of an AK8 PUPPI jet with N or fewer subjets, and is defined as

$$\tau_N = \frac{1}{d_0} \sum_i p_{T,i} \min [\Delta R_{1,i}, \Delta R_{2,i}, \dots, \Delta R_{N,i}], \quad (3)$$

where i is a summation over all jet constituents, d_0 is a normalization constant, and ΔR is the distance between a given jet constituent i and a candidate subjet axis N .

4 Triggers and data set

The events in the dilepton channel are triggered by single-lepton and dilepton triggers without isolation requirements. The triggers for $\mu\mu$ and $e\mu$ events require one muon with $p_T > 50$ GeV and with $|\eta| < 2.4$ that is seeded by hits in either the muon chambers or the inner tracker. The ee events are selected using a dielectron trigger that requires the presence of two electrons with $p_T > 33$ GeV and $|\eta| < 2.5$.

Events used in the single-lepton channel pass either a single electron or a single muon trigger. The single-lepton muon channel uses the same triggers as the dilepton $\mu\mu$ and $e\mu$ channels. The triggers for the electron channel require one electron with $p_T > 115$ GeV or an electron with $p_T > 55$ GeV and a PF jet with $p_T > 165$ GeV. Both triggers require electrons within $|\eta| < 2.5$, and the electron-jet combination trigger requires the jet to be within $|\eta| < 2.4$. In the combination trigger, if the electron lies within the jet footprint, the four-vector of the electron is subtracted from the uncorrected four-vector of the jet, and then the jet energy corrections are reapplied. Neither the muon or electron triggers have isolation requirements.

The fully hadronic analysis uses events that are selected by a logical ‘OR’ of five different triggers. The first trigger requires a single AK8 jet with $p_T > 450$ GeV, a second trigger requires an AK4 jet with $p_T > 360$ GeV and mass (m_{jet}) > 30 GeV. A third trigger requires $H_T > 800$ GeV, where the H_T is the scalar sum of the p_T of every AK4 PF jet above 30 GeV in the event. A fourth trigger requires $H_T > 900$ GeV, and remains un-prescaled during the acquisition of data. The final trigger requires that the $H_T > 700$ GeV, but also requires a jet with $m_{\text{jet}} > 50$ GeV.

Small differences in trigger efficiency between data and simulation in the dilepton and single-lepton channels are accounted for with corrections determined from events selected by triggers with different conditions.

5 Simulated events

The $Z' \rightarrow t\bar{t}$ process is simulated using the MADGRAPH5_aMC@NLO v5.2.2.2 [56] event generator, which produces a resonance with the same spin and left- and right-handed couplings to fermions as the SM Z boson. Matrix element calculations are done at tree level and include up to three additional partons for the g_{KK} and most Z' models, Z' bosons above 5 TeV are simulated with only up to two additional partons in their final state. The $Z' \rightarrow t\bar{t}$ process is simulated at masses between 500 GeV and 7 TeV for resonances with a relative decay width (Γ/m) of 1% (narrow), 10% (wide), and 30% (extra-wide). Matching between the hard matrix element interactions and the lower energy parton showers is done using the MLM algorithm [57]. The KK gluon excitation is simulated using PYTHIA 8.212 [58] with the couplings described in Ref. [59]. The Γ/m of the g_{KK} resonance lies between the wide and extra-wide Z' resonances, depending on its coupling to the top quark. The expected Z' production cross section is calculated at NLO accuracy, and the g_{KK} production cross section is calculated at LO. A multiplicative factor of 1.3 is applied to the g_{KK} cross section as an NLO K factor [60]. Both the Z' and g_{KK} processes are simulated without interference from SM $t\bar{t}$ production.

The invariant mass distribution of the $t\bar{t}$ system at the parton level for Z' resonances with three different widths and a g_{KK} resonance can be seen in Fig. 1. The plots are normalized such that the total integral of each signal model is 1. A resonant structure is manifest at 3 TeV, but at 5 TeV the off-shell component of the signal is strongly enhanced by the available parton luminosity at lower masses. This effect is not noticeable for the narrow Z' signal, but becomes more apparent for the wider Z' resonances. Such behavior is expected for resonant $t\bar{t}$ production in general.

The $t\bar{t}$ pair production background is simulated at next-to-leading order (NLO) with the POWHEG v2 generator [61–64]. The POWHEG generator is also used to simulate single top quark production via EW interactions at NLO [65, 66]. The W +jets background is simulated with the MADGRAPH5_aMC@NLO generator with the FxFx matching prescription between matrix element calculations and parton shower simulations [67]. The Drell–Yan (DY) process with an invariant mass between 10 and 50 GeV is simulated at NLO with the same generator, while for an invariant mass above 50 GeV, leading order (LO) precision is used. Diboson and QCD multijet production are simulated at LO with PYTHIA. It should be noted that simulated multijet events are only used for the background estimate when QCD multijet production is a secondary background. In the case of the fully hadronic analysis, the multijet background is estimated from a CR in data, as described in Section 7.3. For all simulated events, PYTHIA with the CUETP8M1 tune [68] is used to describe the fragmentation and hadronization. All the samples are generated with the NNPDF 3.0 parton distribution functions (PDFs) [69]. All sample cross sections are normalized to the latest theoretical calculations, usually at next-to-NLO precision [70–73].

All samples are processed through a GEANT4-based simulation [74], which models the propagation of the particles through the CMS apparatus and the corresponding detector response. For all samples, the pileup distributions are weighted to have an average of 23 pileup interactions per event, as measured in data. The same event reconstruction software is used for data and simulated events. Differences of a few percent in the resolution and reconstruction efficiency are corrected to match those measured in data using dedicated samples from data [75].

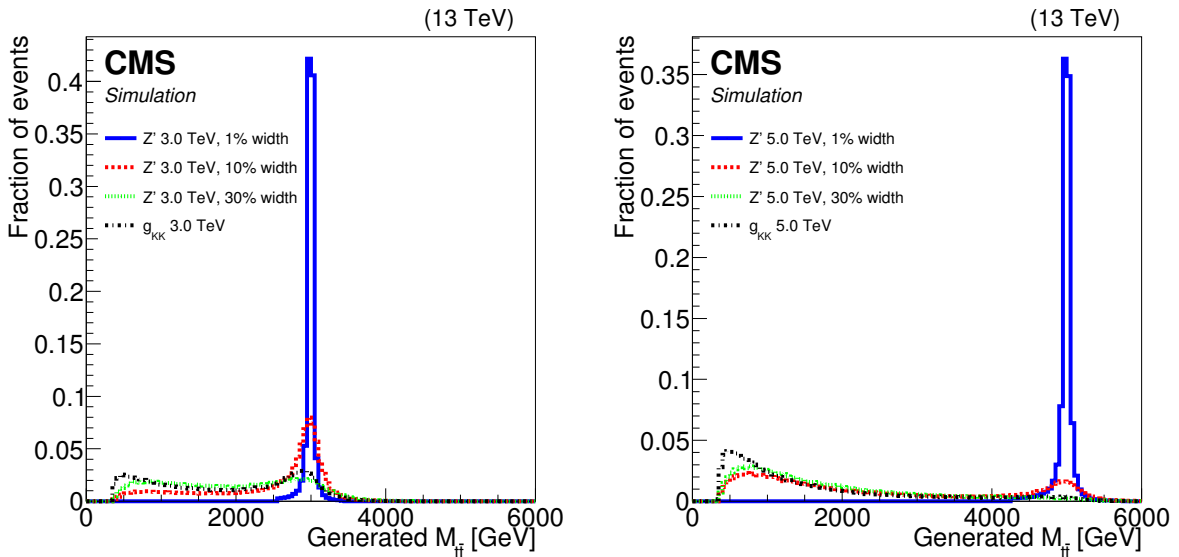


Figure 1: The $t\bar{t}$ invariant mass distributions for four signal models with resonance masses of 3 TeV (left) and 5 TeV (right). The g_{KK} resonance has a relative width $\Gamma/m \approx 15\text{--}20\%$, which is between those of the wide and extra-wide Z' boson signal models.

6 Reconstruction and categorization of $t\bar{t}$ events

6.1 Dilepton channel

Events in the dilepton channel are selected by requiring oppositely charged high- p_T lepton pairs: $\mu\mu$, ee or $e\mu$. Leptons with $p_T > 53$ and 25 (45 and 36) GeV in the $\mu\mu$ (ee) channel are selected. In the $e\mu$ channel, muons are required to have $p_T > 53$ GeV and electrons are required to have $p_T > 25$ GeV. Muons (electrons) are required to be within $|\eta| < 2.4$ (2.5). To remove

contributions from low-mass resonances and $Z/\gamma(\rightarrow \ell\ell)$ +jets production in events with same-flavor lepton pairs, the dilepton invariant mass is required to be above 20 GeV and outside of the Z boson mass window 76 to 106 GeV. Contamination from QCD multijet background is reduced by applying a two-dimensional (2D) selection for both leptons: $\Delta R_{\min}(\ell, j) > 0.4$ or $p_{T,\text{rel}}(\ell, j) > 15$ GeV, where $\Delta R_{\min}(\ell, j)$ is the minimum ΔR -distance between the lepton candidate and any AK4 jet with $p_T > 15$ GeV and $|\eta| < 3$ and $p_{T,\text{rel}}(\ell, j)$ is the p_T of the lepton with respect to the axis of the ΔR -nearest AK4 jet. The 2D selection reduces the QCD multijet background by a factor of ≈ 100 . Events are further required to contain at least two AK4 jets with $|\eta| < 2.4$ and $p_T > 100$ and 50 GeV for the leading and subleading jets, respectively. It is required that at least one of the two leading jets must be b tagged as determined by the loose CSV tagger operating point. Finally, p_T^{miss} is required to be larger than 30 GeV. The resulting sample is dominated by the irreducible $t\bar{t}$ background, which amounts to $>90\%$ of the total background.

Figure 2 shows the distributions of $\Delta R_{\text{sum}} = \Delta R(\ell_1, j) + \Delta R(\ell_2, j)$ in $\mu\mu$, ee , and $e\mu$ subchannels, where $\Delta R(\ell_1, j)$ and $\Delta R(\ell_2, j)$ are the ΔR variables between the leading and subleading lepton and the nearest jet. The lepton-jet pairs from Z' boson decays are expected to be collimated and populate the low- ΔR_{sum} region. The ΔR_{sum} variable is used to separate events into signal- and background-enriched samples: $\Delta R_{\text{sum}} < 1$ and $1 < \Delta R_{\text{sum}} < 2$ defines the boosted and nonboosted signal regions (SRs), respectively, whereas $\Delta R_{\text{sum}} > 2$ defines the background-enriched region. The shape and normalization are in agreement between data and simulation at low ΔR_{sum} , which is the region of interest for separating boosted and resolved events.

6.2 Single-lepton channel

The selection for events used in the single-lepton analysis requires the presence of a muon with $p_T > 55$ GeV and $|\eta| < 2.4$ or an electron with $p_T > 80$ GeV and $|\eta| < 2.5$. Neither lepton has an isolation requirement other than passing the lepton 2D selection, which requires the $\Delta R_{\min}(\ell, j) > 0.4$ or the $p_{T,\text{rel}}(\ell, j) > 25$ GeV, where both quantities are calculated with respect to all AK4 jets with $p_T > 15$ GeV. Events with a second lepton are removed from the sample to avoid any overlap with the dilepton channel. Events are also required to contain at least two AK4 jets with $|\eta| < 2.4$ and a minimum p_T of 150 (185) GeV for the leading jet in the muon (electron) channel, and 50 GeV for the subleading jet. To reduce the contributions to the sample from QCD multijet events, additional requirements are imposed. In the muon channel, p_T^{miss} and H_T^ℓ are required to be greater than 50 and 150 GeV, respectively, where $H_T^\ell \equiv p_T^{\text{miss}} + p_T^\ell$. In the electron channel, it is required that $p_T^{\text{miss}} > 120$ GeV. The electron channel has a higher p_T^{miss} requirement because of the larger QCD multijet background. As a result of this requirement, an additional selection on H_T^ℓ would not increase performance. In order to suppress the contamination from events originating from W+jets events, a boosted decision tree [76] (W+jets BDT) was trained using the TMVA software package [77] on the jet-related variables listed below, in order of importance.

1. $\Delta R_{\min}(\ell, j)$, i.e., the separation between the lepton and its closest jet.
2. The CSV score of the subleading and leading AK4 jets.
3. The number of jets.
4. $p_{T,\text{rel}}(\ell, j)$, i.e., the relative momentum between the jet and nearby lepton.
5. The reconstructed mass of the leading AK4 jet.

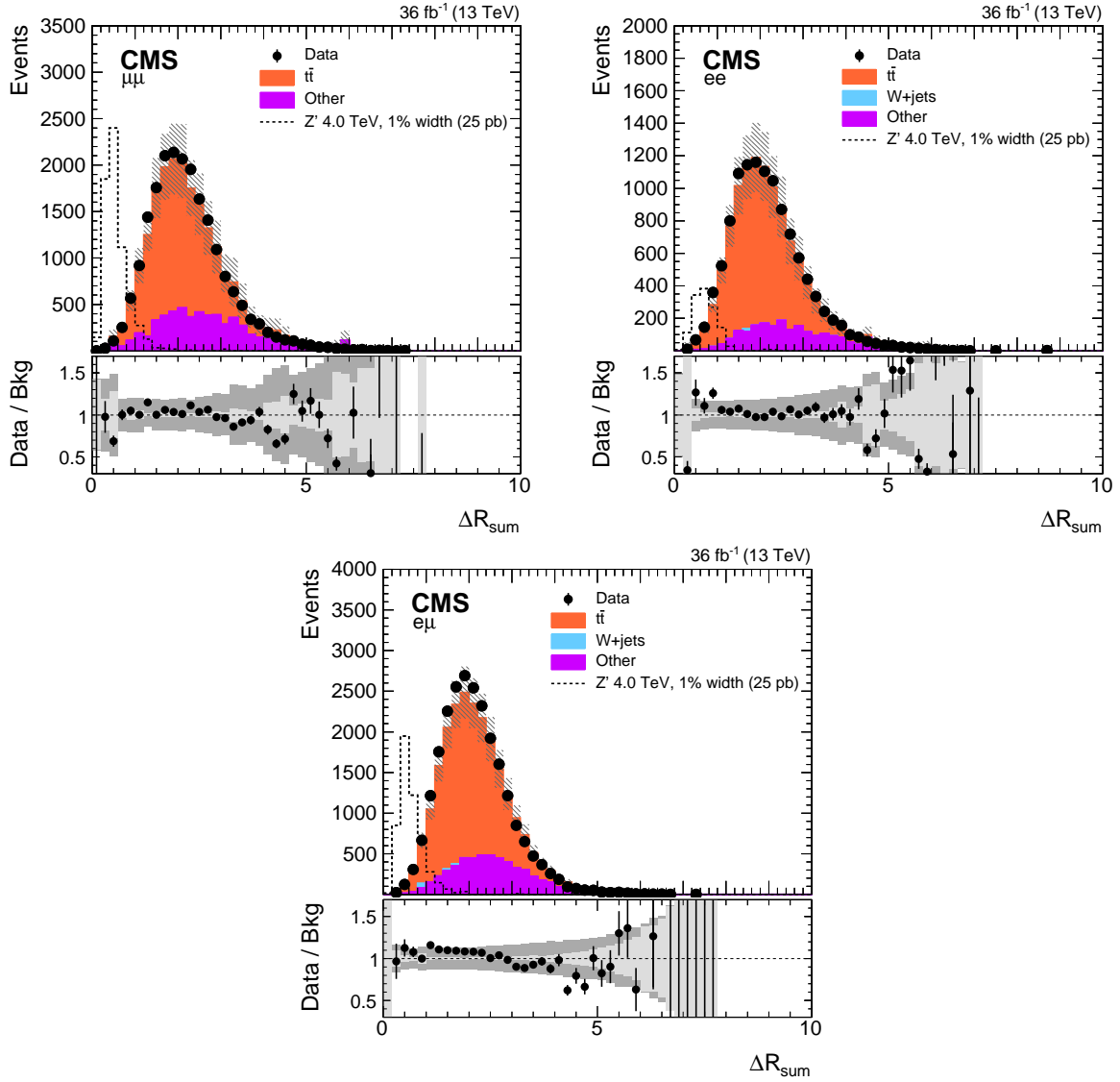


Figure 2: Distributions of ΔR_{sum} in $\mu\mu$ (upper left), ee (upper right), and $e\mu$ (lower) events. The contribution expected from a 4 TeV Z' boson, with a relative width of 1%, is shown normalized to a cross section of 25 pb. The hatched band on the simulated distribution represents the statistical and systematic uncertainties. The lower panels in each plot show the ratio of data to the SM background prediction and the light (dark) gray band represents statistical (systematic) uncertainty. The error bars on the data points indicate the Poisson statistical uncertainties.

6. $\Delta R_{\min}(\ell, j) p_T(j)$, i.e., the ΔR separation between the jet and nearby lepton scaled by the p_T of the jet.
7. The reconstructed mass of the subleading AK4 jet.
8. The shape variable S^{33} of the sphericity tensor $S^{\alpha\beta} = (\sum_i p_i^\alpha p_i^\beta) / (\sum_i |p_i|^2)$, where α, β correspond to the x, y , and z components of the momentum vectors of the jets [78, 79].
9. $H_T + H_T^\ell$, i.e., the summation of the hadronic, leptonic, and p_T^{miss} in the event.

Figure 3 shows the W+jets BDT distribution in the muon and electron channels. The requirement $W\text{+jets BDT} \geq 0.5$ is applied to the events in the SR, which is further separated in two regions, depending on the presence of a t-tagged AK8 jet with $p_T > 400 \text{ GeV}$ and rapidity $|y| < 2.4$. Events with no t-tagged AK8 jet and $W\text{+jets BDT} < -0.75$ or $0 < W\text{+jets BDT} < 0.5$ are dominated by W+jets and $t\bar{t}$ events, respectively, and constitute the background enriched CRs.

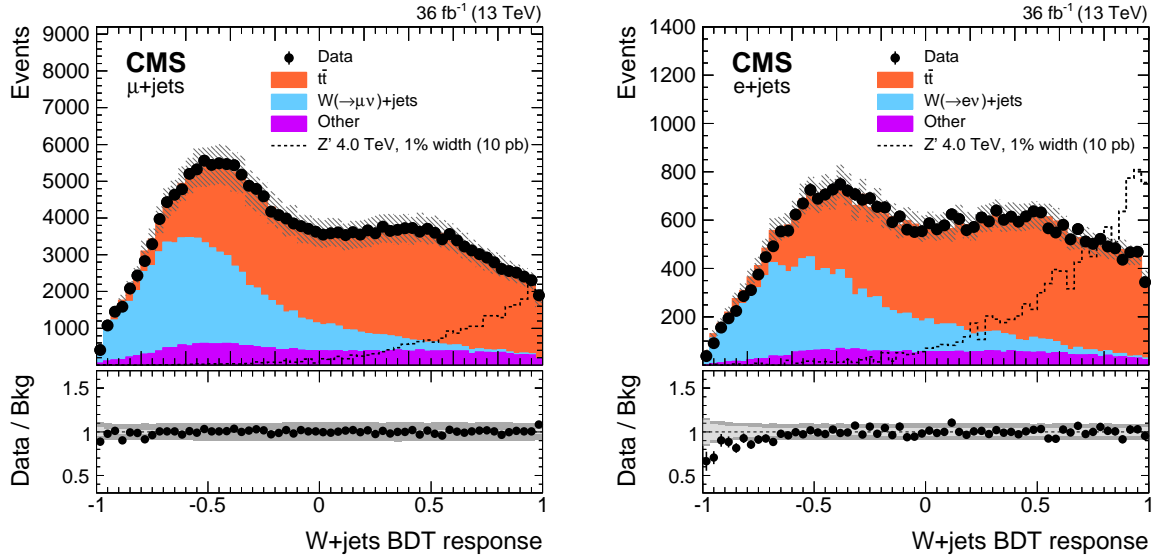


Figure 3: W+jets BDT distributions in the muon (left) and electron (right) single-lepton channel. The SR is defined as events with $W\text{+jets BDT} \geq 0.5$. The contribution expected from a 4 TeV Z' boson, with a relative width of 1%, is shown normalized to a cross section of 10 pb. The hatched band on the simulation represents the statistical and systematic uncertainties. The lower panels in each plot shows the ratio of data to the SM background prediction and the light (dark) gray band represents statistical (systematic) uncertainty. The error bars on the data points indicate Poisson statistical uncertainty.

The $t\bar{t}$ system is reconstructed by assigning the four-vectors of the reconstructed final-state objects (charged lepton, p_T^{miss} , and jets) to the leptonic or hadronic legs of the $t\bar{t}$ decay. For events without an AK8 jet, several hypotheses are built based on possible assignments of each AK4 jet to either the leptonic t decay, the hadronic t decay, or neither. For events with an AK8 jet, that jet is associated with the hadronic t decay, and the leptonic t decay hypotheses only consider AK4 jets that are separated from the AK8 jet by $\Delta R > 1.2$. In both cases, the combination chosen is the one that minimizes the χ^2 discriminator, where

$$\chi^2 = \chi_{\text{lep}}^2 + \chi_{\text{had}}^2 = \left[\frac{m_{\text{lep}} - \bar{m}_{\text{lep}}}{\sigma_{m_{\text{lep}}}} \right]^2 + \left[\frac{m_{\text{had}} - \bar{m}_{\text{had}}}{\sigma_{m_{\text{had}}}} \right]^2. \quad (4)$$

In this equation, m_{lep} and m_{had} are the invariant masses of the reconstructed leptonically and hadronically decaying top quarks, respectively. The parameters \bar{m}_{lep} , $\sigma_{m_{\text{lep}}}$, \bar{m}_{had} , and $\sigma_{m_{\text{had}}}$ in the χ^2 discriminator are determined from simulation by matching reconstructed final-state objects of the hypothesis to the corresponding generator-level particles from the $t\bar{t}$ decay. Events in signal- and background-enriched regions are all required to have $\chi^2 < 30$. Events with two t-tagged AK8 jets are removed from the sample in order to avoid any overlap with the fully hadronic channel.

6.3 Fully hadronic channel

All events used in the fully hadronic analysis are required to fulfill the following kinematic and t tagging criteria. In order to reach a trigger efficiency of $\approx 100\%$, each event must have $H_T > 950$ GeV. Events are reconstructed using the two p_T -leading AK8 jets, both of which are required to have $p_T > 400$ GeV and $|y| < 2.4$. In order to ensure a back-to-back topology, the two jets must have an azimuthal separation $|\Delta\phi| > 2.1$. These kinematic requirements are later referred to as the fully hadronic preselection. Both AK8 jets are required to be t tagged for events to enter the SR. These events are then separated into six SRs based on two criteria: the rapidity difference between the two jets ($|\Delta y| < 1.0$ or $|\Delta y| > 1.0$) and the number of jets with a b-tagged subjet (0, 1, or 2).

The categories with a greater number of jets with a b-tagged subjet are expected to provide higher sensitivity, while those with fewer b-tagged subjets are included to provide better constraints on the backgrounds and additional sensitivity to the analysis. The low- $|\Delta y|$ region is expected to be more sensitive than the high- $|\Delta y|$ region. At high values of $m_{t\bar{t}}$, QCD multijet events will have jets with greater y separation, as compared to those from a massive particle decay, in order to achieve such high invariant masses. This is illustrated in Fig. 4, which shows the dijet rapidity difference for events passing the fully hadronic event selection. The plot on the left is inclusive in $m_{t\bar{t}}$, while the plot on the right shows events with $m_{t\bar{t}} > 2$ TeV.

7 Estimation of the background

7.1 Dilepton channel

The dominant irreducible background in the dilepton channel is $t\bar{t}$ production. Other secondary backgrounds arise from Z+jets, single top quark, and diboson processes. Simulated events are used to model the shape of the kinematic distributions for the background processes, including modeling the S_T variable used in the statistical interpretation of the observations. The overall normalization of the background processes is based on the corresponding theoretical cross sections. The distributions are allowed to vary within prior bounds of rate and shape uncertainties during the statistical treatment, which employs six signal- and three background-enriched regions, defined in Section 6.1. Modeling of the background is separately checked in the background-enriched CR obtained with the requirement $\Delta R_{\text{sum}} > 2$. Figure 5 shows the distributions of S_T in the CR for $\mu\mu$, ee , and $e\mu$ channels. The background simulation is in agreement with data within the statistical and systematical uncertainties. The quantity ‘pull’, shown in Fig. 5 and subsequent figures, is computed according to the following procedure. First, the total uncertainty per bin is determined by adding the statistical and all systematic uncertainties together in quadrature. Based on the expected number of events and the total uncertainty in each bin, pseudo-experiments are performed by sampling from a Gaussian distribution with the mean equal to the expected number of events and the standard deviation equal to the total uncertainty. For each pseudo-experiment, a distribution of the number of

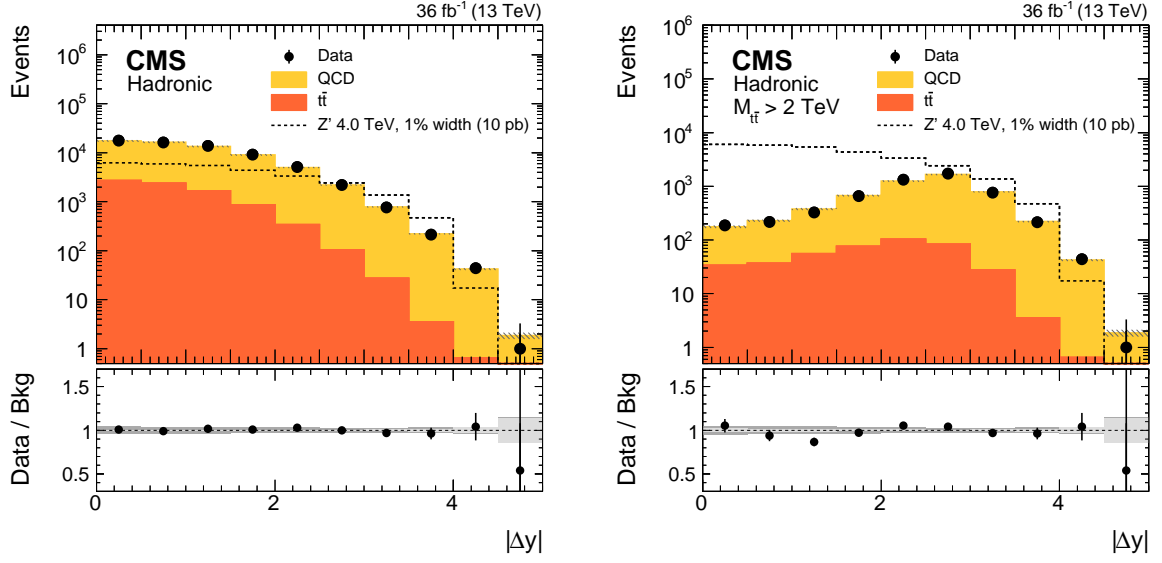


Figure 4: Dijet rapidity difference (Δy) for events passing the fully hadronic event selection for all $m_{t\bar{t}}$ (left) and for events with an $m_{t\bar{t}} > 2$ TeV (right). The contribution expected from a 4 TeV Z' boson, with a relative width of 1%, is shown normalized to a cross section of 10 pb. The hatched band around the simulated distribution represents the statistical and systematic uncertainties. The lower panels in each plot show the ratio of data to the SM background prediction and the light (dark) gray band represents statistical (systematic) uncertainty.

expected events is populated using Poisson statistics convolved with the Gaussian distribution describing the variation in the expected number of events in the bin. Finally, the number of events observed in data is used in conjunction with the distribution of pseudo-experiments to calculate a p-value, and the corresponding z-score is taken to be the pull.

7.2 Single-lepton channel

Standard model $t\bar{t}$ production is the main irreducible background in the single-lepton channel. Other background processes include W +jets, single top quark, Z +jets, and diboson production. The QCD multijet background is a minor contribution in the single muon channel ($\approx 3\%$), and is suppressed to a negligible level in the single-electron channel because of higher p_T and p_T^{miss} requirements. All background processes in the single-lepton channel are modeled from simulated events, and the normalization of each background is based on its theoretical cross section. The rate and shape of the backgrounds are allowed to vary in the statistical analysis as described in Section 9. Events that pass the requirements in Section 6.2 are separated in two signal- and two background-enriched regions, defined as follows.

1. Signal Region (SR1T): $\chi^2 < 30$, W +jets BDT ≥ 0.5 , 1 t-tagged AK8 jet.
2. Signal Region (SR0T): $\chi^2 < 30$, W +jets BDT ≥ 0.5 , no t-tagged AK8 jet.
3. Control Region (CR1): $\chi^2 < 30$, W +jets BDT < -0.75 .
4. Control Region (CR2): $\chi^2 < 30$, $0.0 < W$ +jets BDT < 0.5 .

The first control region (CR1) is dominated by W +jet events, while CR2 is dominated by $t\bar{t}$ events. For all regions, events are separated based on the lepton flavor (μ , e), which results

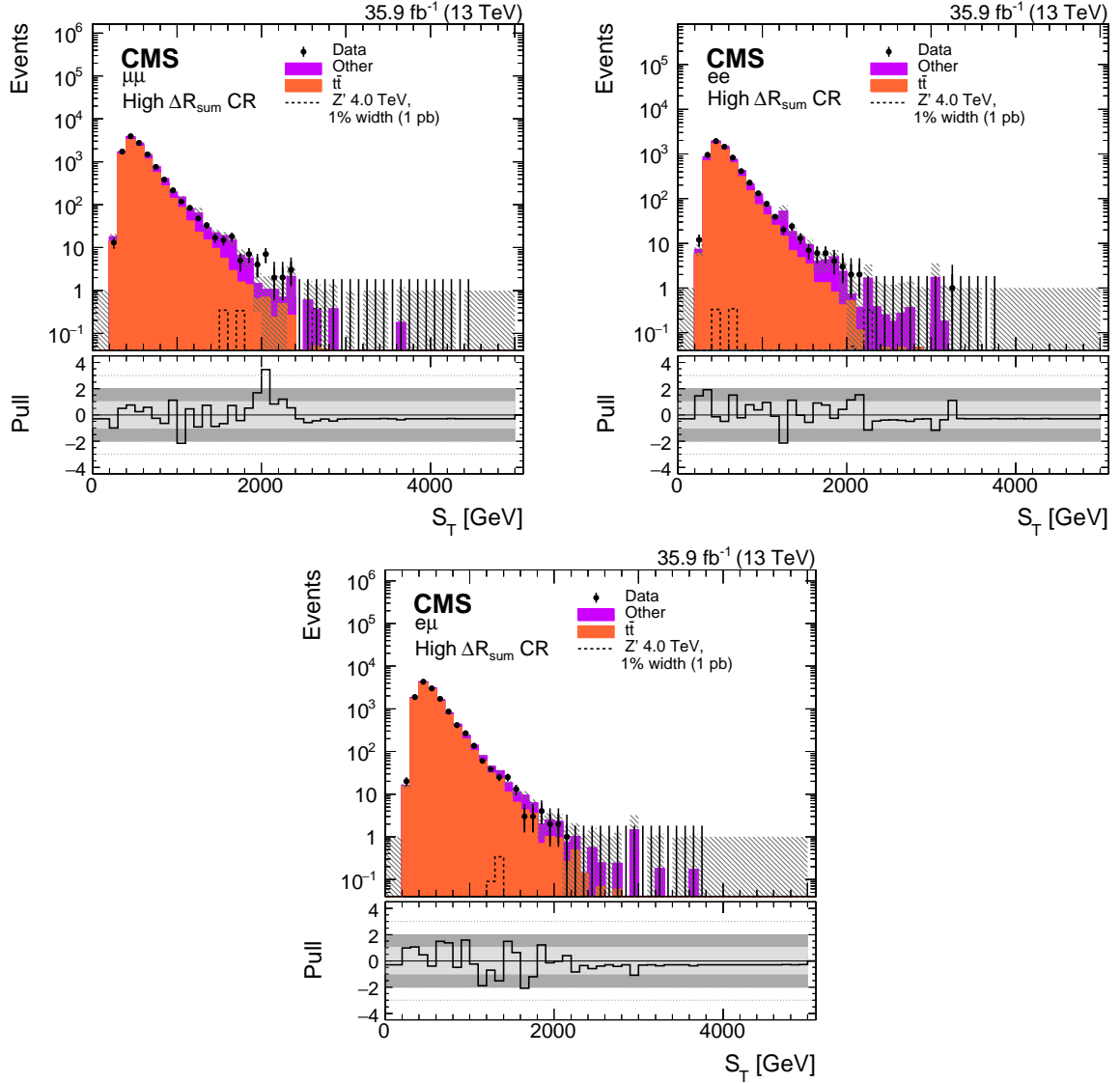


Figure 5: Distributions of S_T in the background-enriched CR for $\mu\mu$ (upper left), ee (upper right), and $e\mu$ (lower) subchannels. The contribution expected from a 4 TeV Z' boson, with a relative width of 1%, is shown normalized to a cross section of 1 pb. The hatched band on the simulation represents the uncertainty in the background prediction. The lower panel shows the pull of each histogram bin from the SM prediction. The light (dark) gray band represents a pull of one (two) standard deviations (s.d.) from the predicted value.

in eight exclusive categories used in the binned maximum likelihood fit. The rate at which light-flavor quarks and gluons are misidentified as originating from top quarks (t mistag) is measured in data and simulation using a W +jets mistag CR with $\chi_{\text{lep}}^2 > 30$ and W +jets BDT < -0.5 . The p_T and m_{SD} distributions in the W +jets background can be seen in Fig. 6.

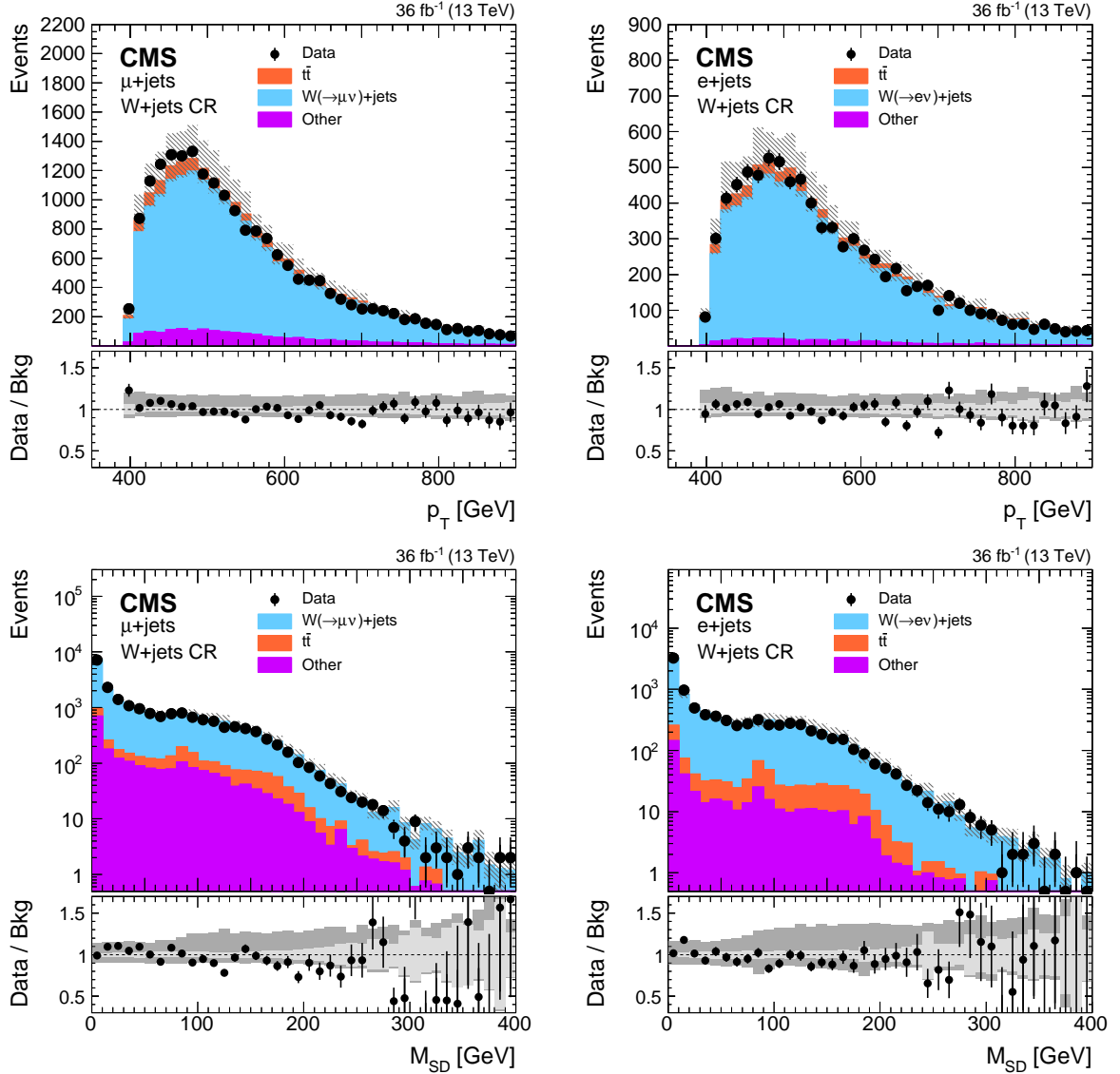


Figure 6: Distributions of p_T (upper) and m_{SD} (lower) for the W +jets background in the muon (left) and electron (right) channels using the W +jets mistag CR. The jet p_T information is taken from the CHS jets, while the m_{SD} is taken from the PUPPI jets. The hatched band on the simulation represents the uncertainty in the background prediction. The lower panels in each plot show the ratio of data to the SM background prediction and the light (dark) gray band represents statistical (systematic) uncertainty.

7.3 Fully hadronic channel

The two main sources of background in the fully hadronic channel are QCD multijet and $t\bar{t}$ production. For the latter background, simulated events are used to model the shape of the $m_{t\bar{t}}$ distribution. This distribution is initially normalized to the theoretical cross section, but it is allowed to vary within the bounds of rate and shape uncertainties during the statistical

treatment. The final normalization and shape are determined by fitting the distributions in the six SRs, defined in Section 6.3.

The QCD multijet background is estimated from data, using a method similar to the techniques described in Ref. [30]. The preselection described in Section 6.3 is enforced in order to select a back-to-back dijet event topology. In the first step of the background estimate, the t mistag rate in QCD multijet events is measured. A QCD multijet enriched region is selected by requiring one of the two jets to be “anti-tagged,” meaning it has a PUPPI soft drop mass in the t -tag mass window $105 < m_{SD} < 210$ GeV, but the N -subjettiness requirement is inverted to $\tau_{32} > 0.65$. The opposite “probe” jet is used to determine the t mistag rate. This rate is parametrized as a function of probe jet momentum (p) and is measured for each of the three subjet b -tag categories (Fig. 7). This “anti-tag and probe” procedure is repeated for the $t\bar{t}$ simulation, indicating that there is a small ($\approx 2\%$) contribution from SM $t\bar{t}$ events. The observed $t\bar{t}$ contamination is then subtracted from the anti-tag and probe data selection.

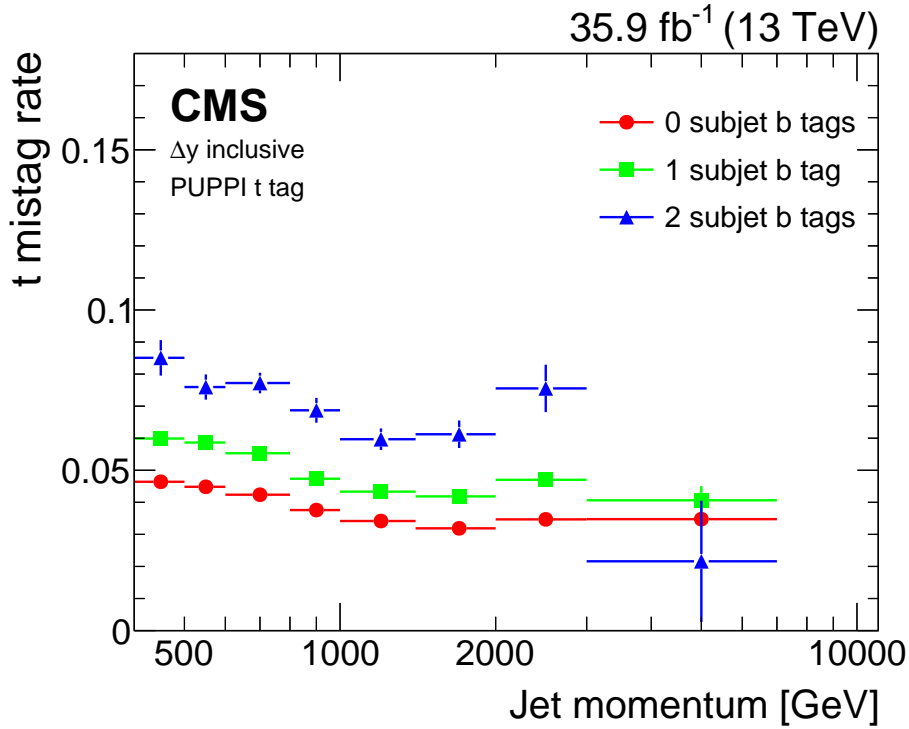


Figure 7: The t mistag rate as measured with an anti-tag and probe procedure separately for each b -tag category.

After the t mistag rate has been measured in the QCD multijet CR, it is used to estimate the $m_{t\bar{t}}$ QCD multijet distribution in the SR. First, a “single-tagged” region is selected, in which at least one of the two jets is required to be t tagged, meaning it has a PUPPI m_{SD} in the t -tag mass window $105 < m_{SD} < 210$ GeV and an N -subjettiness requirement of $\tau_{32} < 0.65$. One of the two top quark jet candidates is randomly selected, in order to avoid bias. If the selected jet is t tagged, the event is included in the QCD multijet estimate. The event is weighted by the previously measured t mistag rate, based on the momentum of the opposite jet and the number of subjet b tags in the event. Again, the procedure is repeated for the $t\bar{t}$ simulation, and the $t\bar{t}$ contamination is subtracted from the QCD multijet background estimate. This eliminates double counting between the $t\bar{t}$ and QCD multijet distributions.

Finally, a “mass-modified” procedure is employed in order to ensure that the jets used in the

QCD multijet estimate mimic the relevant kinematics of the jets in the SR. If the mass of the second QCD multijet jet is not in the top quark mass window, it is assigned a random value within that window. This modified mass is randomly selected from the distribution of simulated light-flavor jets, with masses within the t-tag window, $105 < m_{SD} < 210$ GeV. A check of the entire background estimation method using simulated QCD multijet events is self-consistent.

8 Systematic uncertainties

Several sources of uncertainty that impact the final results of this search are considered. In all cases, the uncertainties in reconstruction efficiency and event interpretation are propagated to the distribution used for signal extraction. These uncertainties can be broadly grouped into two categories: those uncertainties that affect only the overall normalization of expected background events and those uncertainties that can result in a different reconstruction of the $t\bar{t}$ system, and therefore change the shape of the $m_{t\bar{t}}$ distribution. Each source of systematic uncertainty is accounted for through unique nuisance parameters applied to the likelihood described in Section 10. For contributions that apply to multiple analysis channels, the nuisance parameters are fully correlated, allowing better constraints to be placed on sources of systematic uncertainties. The individual sources of uncertainty are described in detail below, and are summarized in Table 1.

Including all the systematic uncertainties degrades the final cross section limits by 10% for resonance masses above 2.5 TeV. Lower mass hypotheses are more sensitive to the systematic effects, thus the limit on the cross section degrades by up to 60% for the lowest mass Z' resonance considered (500 GeV). The uncertainties in the jet energy corrections, pileup distribution, and $t\bar{t}$ cross section are the most significant. They result in a reduction of the excluded mass by 1.1, 1.0, and 1.0%, respectively. All other systematic uncertainties have less than a 1% effect. Per channel, the most significant systematic uncertainties are the b tagging scale factor, the $t\bar{t}$ renormalization and factorization scales, and the standard model $t\bar{t}$ cross section for the dilepton, single-lepton, and all hadronic channels, respectively. The most constrained nuisance parameters are those associated with the $t\bar{t}$ renormalization and factorization scales as well as the top tagging efficiency, which are constrained to 8.5 and 9.2% of their prior uncertainty. The average nuisance parameter has a post-fit uncertainty that is 75% lower than its prior estimate.

1. *Standard model cross sections*: Uncertainties in the cross sections used to normalize simulated background processes are obtained using the fitting procedure described in Section 1. For the $t\bar{t}$, W +jets, and Z +jets backgrounds, a priori uncertainties of 20, 25, and 50% are assigned, respectively. A cross section uncertainty of 50% is used for the subdominant diboson and single top quark backgrounds. The values chosen reflect the relatively large uncertainties associated with modeling these backgrounds in the Lorentz-boosted phase space where the analysis is performed.
2. *Integrated luminosity*: The uncertainty in the measurement of the integrated luminosity is 2.5% [80], and is applied to all simulated signal and background samples.
3. *Pileup reweighting*: All simulated samples used in the analysis are reweighted to ensure that the distribution of the number of pileup interactions per event matches the corresponding distribution in data. This pileup distribution is obtained using a total inelastic cross section value of 69.2 mb [81, 82]. A systematic uncertainty in the distribution is obtained by varying the value by $\pm 4.6\%$, which is calculated using the method described in [82] using the cross sections from [81]. The resulting uncertainty has both a normalization and shape component.

Table 1: Sources of systematic uncertainty that affect the $m_{t\bar{t}}$ and S_T distributions in each analysis channel. For uncertainty sources that apply to multiple channels, the corresponding nuisance parameter is fully correlated across these channels if the symbol \checkmark appears in the same row. For normalization uncertainties, the size of the effect on the prior distribution is indicated. Shape uncertainties have priors of ± 1 s.d., and the dependence on the kinematic quantities is shown.

Source	Uncertainty	Prior	Channel		
			Dilepton	Single-Lepton	Hadronic
b tagging efficiency		± 1 s.d. (p_T, η)	\checkmark		\checkmark
b mistag rate		± 1 s.d. (p_T, η)	\checkmark		\checkmark
Parton distribution functions		± 1 s.d.	\checkmark	\checkmark	\checkmark
CSV discriminator shape		± 1 s.d.		\checkmark	
Diboson cross section		50%	\checkmark		
Electron trigger		± 1 s.d. (p_T, η)	\checkmark	\checkmark	
Electron identification		± 1 s.d. (p_T, η)	\checkmark	\checkmark	
Jet energy scale		± 1 s.d. (p_T, η)	\checkmark	\checkmark	\checkmark
Jet energy resolution		± 1 s.d. (η)	\checkmark	\checkmark	\checkmark
Integrated luminosity measurement		2.5%	\checkmark	\checkmark	\checkmark
QCD multijet modified mass procedure		± 1 s.d.			\checkmark
QCD multijet estimate closure test		± 1 s.d.			\checkmark
Muon trigger		± 1 s.d. (p_T, η)	\checkmark	\checkmark	
Muon identification		± 1 s.d. (η)	\checkmark	\checkmark	
Pileup reweighting		± 1 s.d.	\checkmark	\checkmark	\checkmark
Renorm/fact. scales ($t\bar{t}$ production)		± 1 s.d.	\checkmark	\checkmark	\checkmark
Single top quark cross section		50%	\checkmark		
t tagging efficiency		unconstrained		\checkmark	\checkmark
t mistag rate (fully hadronic)		± 1 s.d. (p)			\checkmark
t mistag rate (single-lepton)		± 1 s.d.		\checkmark	
Top quark pair cross section		20%	\checkmark	\checkmark	\checkmark
Top quark p_T reweighting		± 1 s.d.	\checkmark	\checkmark	\checkmark
W+jets cross section		25%	\checkmark	\checkmark	
Z+jets cross section		50%	\checkmark	\checkmark	

-
4. *Lepton reconstruction and triggers*: Simulated events are corrected by scale factors to account for differences between data and simulation in the efficiencies in the identification criteria for muons and electrons. By applying the scale factors shifted up or down by their uncertainties, new templates are obtained that correspond to these uncertainties. These templates can be used as the nuisance parameters, which are correlated between channels as identical identification criteria are used. The scale factors are parametrized as functions of lepton p_T and η to account for different detector response. In the same way, uncertainties in the trigger efficiency are also accounted for, in the muon and electron trigger selections for this analysis.
 5. *Jet energy scale and resolution*: Uncertainties in the energy corrections applied to jets are propagated to the final discriminating distributions by reconstructing events with the jet level corrections shifted within their corresponding uncertainties, which depend on the jet p_T and η .
 6. *Jet b tagging*: Simulated events are corrected with scale factors to account for differences in the efficiency for identifying a b jet between data and simulation. There are two components to this process, each with an independent, uncorrelated nuisance parameter: one that accounts for the scale factor applied to the rate of identifying b-tagged jets (efficiency) and one that accounts for the scale factor applied to the rate of mistakenly identifying light-flavor jets as b jets (b mistag rate). In each case, the uncertainty is obtained by shifting these p_T -dependent scale factors within their uncertainties. The b tagging uncertainties are fully correlated between the dilepton and fully hadronic analyses, as they use the same b tagging criteria.
 7. *CSV discriminant shape*: The CSV tagger provides a continuous variable that can be used to identify b jets. This continuous variable is used as an input to the W+jets BDT described above. The W+jets BDT is only used in the single-lepton analysis, therefore the CSV shape systematic uncertainty only applies to that analysis. Several sources of systematic uncertainties are evaluated, including jet energy scale, flavor effects, and statistical effects. Each of these effects contributes an additional uncertainty in the CSV value that is propagated to the final signal discrimination process.
 8. *Jet t tagging*: It is not possible to define a CR that is capable of measuring the t tagging scale factor without overlapping the $t\bar{t}$ SR. The t tagging efficiency scale factor is determined during the statistical analysis. This is done by including a nuisance parameter with a flat prior distribution that is unconstrained and correlated between the fully hadronic and single-lepton channels. Sources of misidentified t-tagged jets are different in the single-lepton channel, where they originate from W+jets processes, and in the fully hadronic channel, where they originate from QCD multijet processes. Therefore, the nuisance parameters corresponding to the uncertainty in the t mistag rate are treated as uncorrelated between the channels, and are also uncorrelated with the nuisance parameter assigned to the t tagging efficiency.
 9. *Parton distribution functions*: For the $t\bar{t}$ simulated sample, the PDFs from the NNPDF3.0 set [69] are used to evaluate the systematic uncertainty in the choice of PDF, according to the procedure described in Ref. [83].
 10. *Scale uncertainties*: For the $t\bar{t}$ sample, the matrix element renormalization and factorization scales were varied up and down independently by a factor of 2 to account for uncertainties in the choice of Q^2 used to generate the simulated sample.

11. *Top quark p_T reweighting*: The simulated SM $t\bar{t}$ process was corrected at parton-level using a function derived from the ratio of top quark p_T measured in data and next-to-NLO predictions from POWHEG and PYTHIA [84]. The uncertainty in this process is estimated by taking the difference between the unweighted and weighted results applied symmetrically to the nominal value as a function of p_T . The top quark p_T reweighting does not significantly impact the $m_{t\bar{t}}$ and S_T distributions, and would not obscure a resonance signal.
12. *QCD multijet background estimation*: The ‘mass-modified’ procedure described above to predict the shape of the background in the fully hadronic channel includes an uncertainty in the resulting distribution, equivalent to half of the difference between the uncorrected and ‘mass-modified’ background shapes. This difference affects both the shape and normalization of the final distributions, and the corresponding nuisance parameter is independent from all other effects. The uncertainties in the t mistag rates are propagated to the final distributions, and the corresponding uncertainty is handled via the t mistag rate nuisance parameter described above. A closure test is performed with simulated QCD multijet events to test the accuracy of the method. An additional systematic uncertainty is included, equal to the magnitude of the discrepancy observed from the closure tests results, evaluated and applied on a bin-by-bin basis to the fully hadronic signal categories. This systematic most greatly affects the two b-tag, high- $|\Delta y|$ category, for which the method only closes within 20%. For the other categories, the method closes within $\approx 4\%$.

9 Statistical analysis

Before extracting the final results of the analysis, a background-only binned maximum likelihood fit is performed on the signal and control regions to determine the preferred values of the background process normalizations and shapes, using constraints from the sources of systematic uncertainty described above. Each source of systematic uncertainty is included through a unique nuisance parameter that is allowed to vary within the rate and shape constraints described above, using a log-normal prior distribution. The post-fit values of the nuisance parameters are used to correct the normalization and shape of each background process. The $m_{t\bar{t}}$ and S_T distributions after the fitting procedure are shown in Figs. 8, 9–10, and 11, for the dilepton, single-lepton, and fully hadronic channels, respectively. The mild deficits at low $m_{t\bar{t}}$ in the two plots on the left in Fig. 10 do not significantly impact the limit, because this region is used to evaluate the $t\bar{t}$ and W +jets cross sections and is not sensitive to the resonance signal. The t tagging efficiency is measured simultaneously in signal and control regions during the maximum likelihood fit, as it is not possible to select a CR that might not be contaminated by the potential signal. The t tagging efficiency scale factor is modeled as a free nuisance parameter, with an unconstrained prior, in the binned likelihood fit. The t tagging efficiency scale factor measured by the fit is 1.001 ± 0.012 .

Data are found to be in agreement with expectations in each of the categories considered in this analysis. Limits on the product of the production cross section and branching fraction are calculated, $\sigma(pp \rightarrow X) \mathcal{B}(X \rightarrow t\bar{t})$, for heavy resonances decaying to a pair of top quarks. A shape-based analysis is performed using both the signal and control regions from the three exclusive analysis channels. The THETA software package [85] simultaneously fits the $m_{t\bar{t}}$ distributions from the single-lepton and fully hadronic channels and the S_T distributions from the dilepton channel. For the limit calculation, a Bayesian likelihood-based method is used [86, 87] with each bin of the distributions combined statistically, along with the implementation of

unique nuisance parameters that correspond to the systematic uncertainties described in Section 8. The signal normalization is allowed to vary with a distinct unconstrained nuisance parameter having a uniform prior, while the other nuisance parameters have log-normal prior distributions. Finally, to account for the limited number of simulated events, an additional statistical uncertainty is included for each process relying on simulated events through the “Barlow–Beeston lite” method [88]. Prior to the statistical analysis, the $m_{t\bar{t}}$ distributions are rebinned. For the fully hadronic and dilepton channels, the total statistical uncertainty in the background is required to be below 30% in any given bin. In the single-lepton channel, the total statistical uncertainty in the background expectation for the sum of small backgrounds (single top quark, multijet, Z+jets, W + b, or c jets) is required to be below 10% in each bin. The tighter statistical uncertainty requirement is needed for these backgrounds because the events are rejected at a high rate, resulting in significantly fewer simulated events that pass the final selection.

Figure 12 shows a comparison of the expected sensitivities in each of the three analysis channels in terms of the expected limits for the g_{KK} signal model. The contributions from the single-lepton and fully hadronic channels dominate the sensitivity over most of the mass range, apart from the region of lowest masses, where the dilepton channel makes a significant contribution.

10 Results

The statistical analysis is performed for each of the signal models considered in this analysis: three variations of a Z' boson having a width-to-mass ratio of 1, 10, and 30%, as well as a g_{KK} . In each case, a 95% CL limit is obtained on the product of the resonance production cross section and branching fraction. The observed and expected limits and 1 and 2 s.d. bands are calculated for resonance masses ranging from 0.5 to 5.0 TeV and are listed in Tables 2–5.

Table 2: Limits at 95% CL on the product of the resonance production cross section and branching fraction for the narrow ($\Gamma/m = 1\%$) Z' boson resonance hypothesis.

Mass [TeV]	Obs. [pb]	Median exp. [pb]	68% Exp. [pb]	95% Exp. [pb]
0.50	29	28	[13, 49]	[7.5, 78]
0.75	1.1	2.4	[1.5, 3.7]	[1.0, 5.6]
1.00	0.37	0.54	[0.37, 0.77]	[0.26, 1.1]
1.25	0.31	0.16	[0.11, 0.24]	[0.080, 0.35]
1.50	0.091	0.076	[0.051, 0.12]	[0.036, 0.17]
2.00	0.023	0.027	[0.018, 0.041]	[0.012, 0.061]
2.50	0.018	0.012	[0.0083, 0.019]	[0.0056, 0.029]
3.00	0.0042	0.0075	[0.0051, 0.011]	[0.0035, 0.017]
3.50	0.0046	0.0052	[0.0035, 0.0081]	[0.0025, 0.012]
4.00	0.0041	0.0042	[0.0028, 0.0065]	[0.0020, 0.010]
4.50	0.0030	0.0035	[0.0023, 0.0054]	[0.0016, 0.0082]
5.00	0.0023	0.0032	[0.0021, 0.0049]	[0.0014, 0.0079]
6.00	0.0013	0.0027	[0.0017, 0.0042]	[0.0011, 0.0069]
6.50	0.0012	0.0026	[0.0016, 0.0040]	[0.0011, 0.0065]
7.00	0.0012	0.0024	[0.0016, 0.0038]	[0.0011, 0.0063]

New exclusion limits on the mass of resonances decaying to $t\bar{t}$ are set by comparing the observed limit to the theoretical cross section, where the branching fraction $\mathcal{B}(X \rightarrow t\bar{t})$ is assumed to be 1. As shown in Fig. 13, the analysis excludes narrow Z' bosons with masses up to 3.80 TeV (3.75 TeV expected), wide Z' bosons with masses up to 5.25 TeV (5.10 TeV expected), and extra-

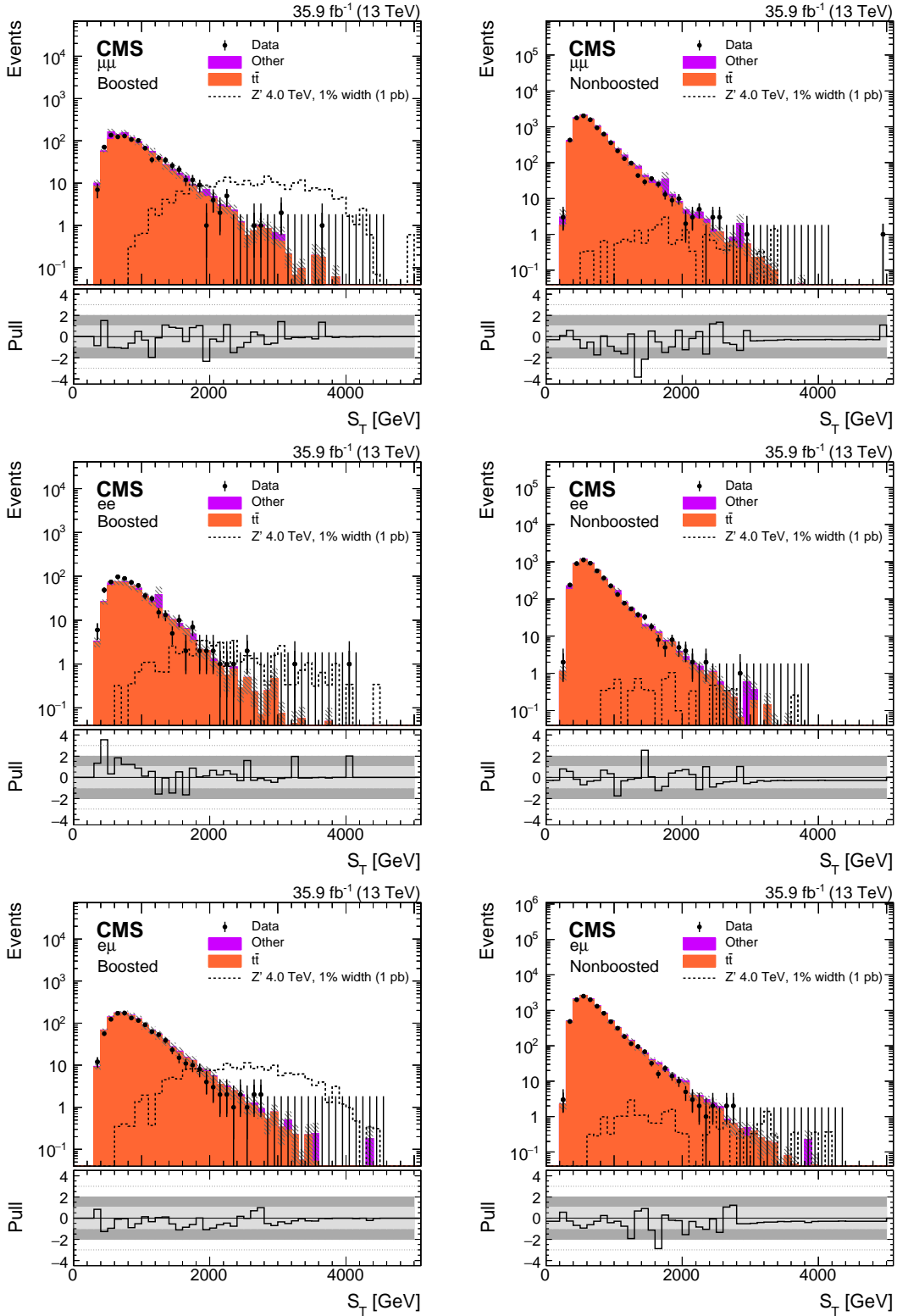


Figure 8: Distributions of S_T for the $\mu\mu$ (upper), ee (middle), and $e\mu$ (lower) SRs in the boosted (left) and nonboosted (right) regions, as defined in Section 6.1. The contribution expected from a 4 TeV Z' boson, with a relative width of 1%, is shown normalized to a cross section of 1 pb. The hatched band on the simulation represents the uncertainty in the background prediction. The lower panel in each plot shows the pull of each histogram bin from the SM prediction. The light (dark) gray band represents a pull of one (two) s.d. from the predicted value.

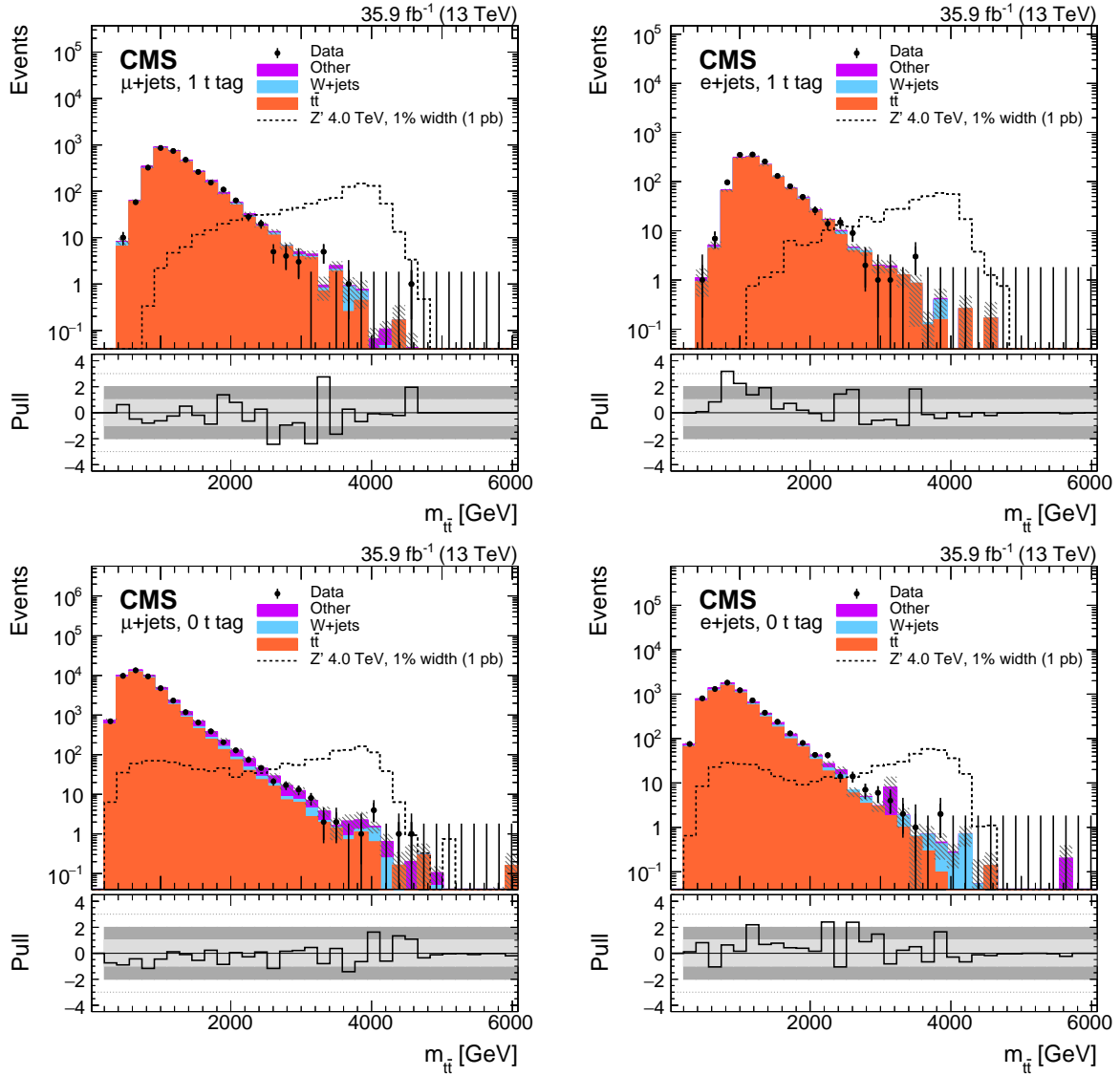


Figure 9: Distributions of $m_{t\bar{t}}$ for the single-lepton channel SRs for the muon (left) and electron (right) categories with (upper) and without (lower) t tagging. The contribution expected from a 4 TeV Z' boson, with a relative width of 1%, is shown normalized to a cross section of 1 pb. The hatched band on the simulation represents the uncertainty in the background prediction. The lower panel in each plot shows the pull of each histogram bin from the SM prediction. The light (dark) gray band represents a pull of one (two) s.d. from the predicted value.

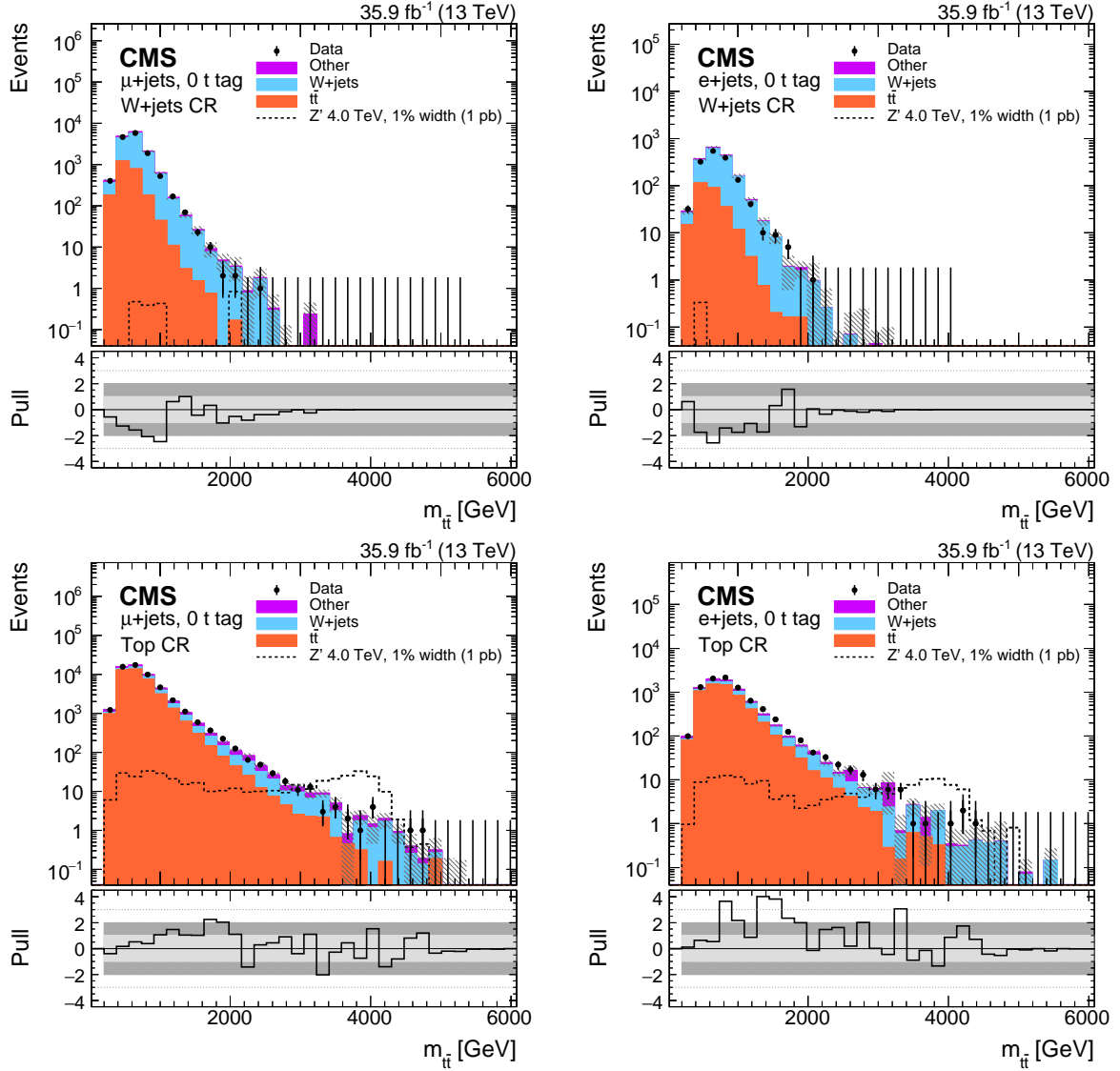


Figure 10: Distributions of $m_{\bar{t}t}$ for the single-lepton channel CR1 (upper) and CR2 (lower) for the muon (left) and electron (right) categories. The contribution expected from a 4 TeV Z' boson, with a relative width of 1%, is shown normalized to a cross section of 1 pb. The hatched band on the simulation represents the uncertainty in the background prediction. The lower panel in each plot shows the pull of each histogram bin from the SM prediction. The light (dark) gray band represents a pull of one (two) s.d. from the predicted value.

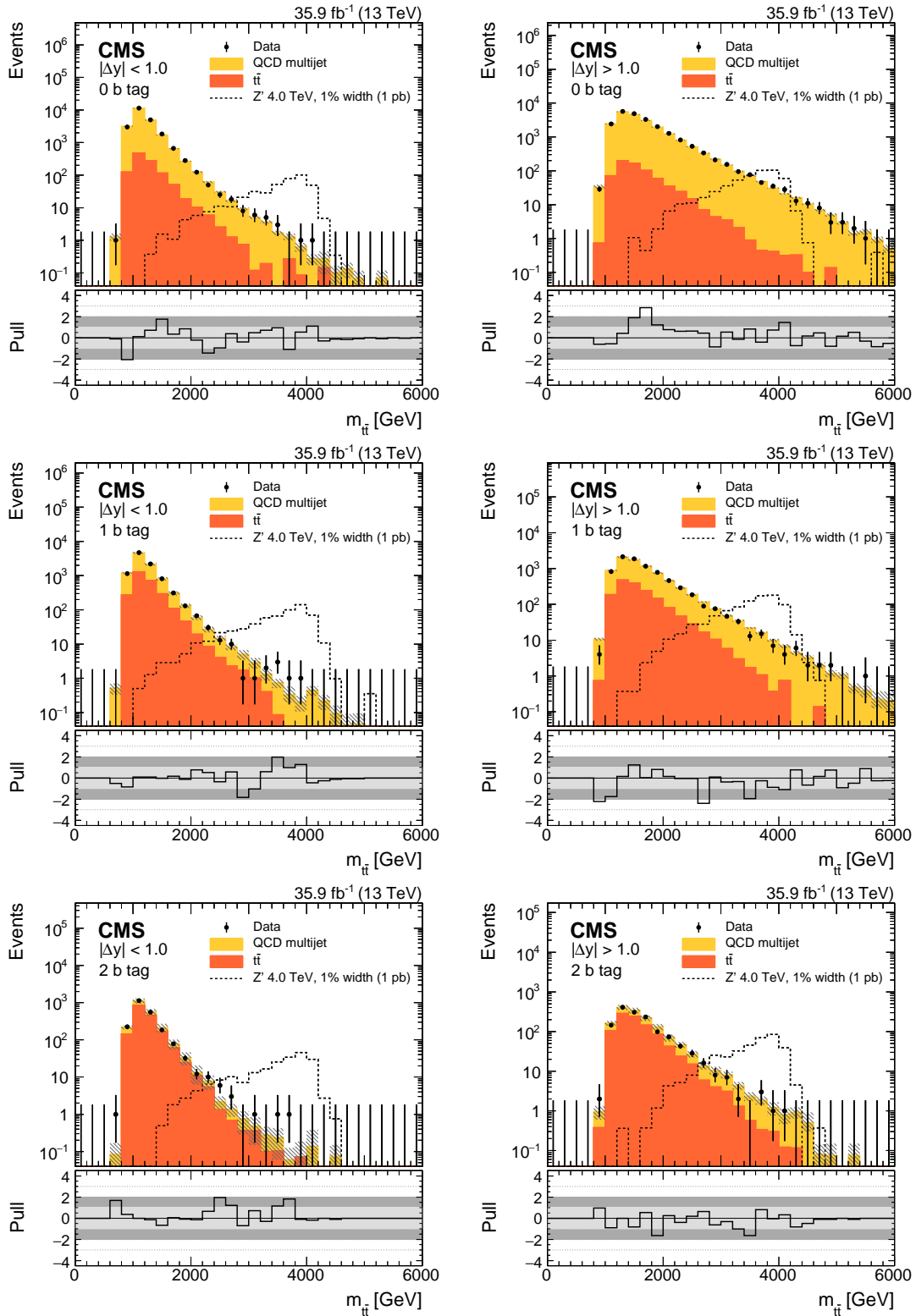


Figure 11: Distributions of $m_{\bar{t}t}$ for the fully hadronic channel SR categories, used to extract the final results. The contribution expected from a 4 TeV Z' boson, with a relative width of 1%, is shown normalized to a cross section of 1 pb. The hatched band on the simulation represents the uncertainty in the background prediction. The lower panel in each plot shows the pull of each histogram bin from the SM prediction. The light (dark) gray band represents a pull of one (two) s.d. from the predicted value.

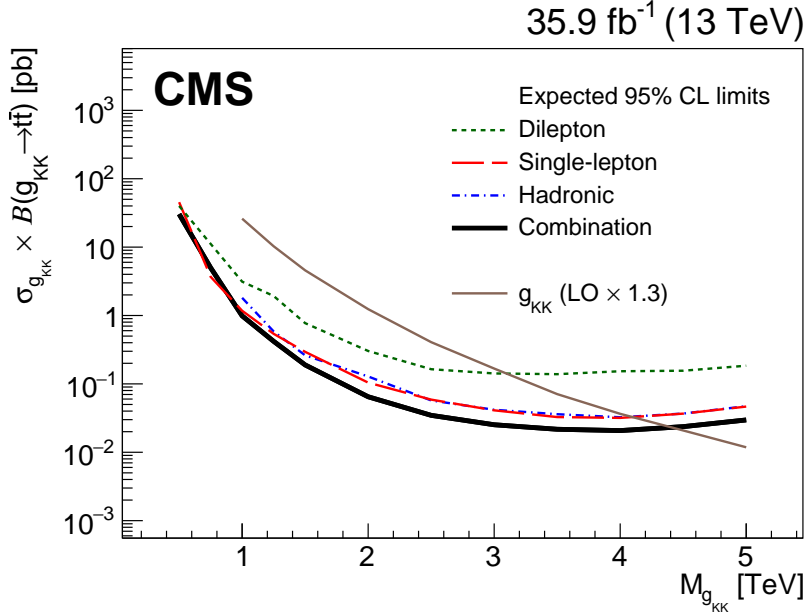


Figure 12: Comparison of the sensitivities for each analysis channel contributing to the combination. The expected limits at 95% CL are shown for each channel with the narrow colored lines, while the combination result is shown with thick the black line. These results are shown specifically for the g_{KK} signal hypothesis, as this model has characteristics that are common to many $t\bar{t}$ resonance searches. The multiplicative factor of 1.3 for the g_{KK} is the NLO K factor.

Table 3: Limits at 95% CL on the product of the resonance production cross section and branching fraction for the wide ($\Gamma/m = 10\%$) Z' boson resonance hypothesis.

Mass [TeV]	Obs. [pb]	Median exp. [pb]	68% Exp. [pb]	95% Exp. [pb]
0.50	31	22	[9.8, 43]	[5.4, 70]
0.75	2.9	3.6	[2.2, 6.1]	[1.3, 9.5]
1.00	0.93	0.72	[0.48, 1.1]	[0.34, 1.5]
1.25	0.55	0.24	[0.16, 0.37]	[0.11, 0.54]
1.50	0.17	0.12	[0.073, 0.18]	[0.050, 0.29]
2.00	0.041	0.040	[0.027, 0.063]	[0.018, 0.096]
2.50	0.027	0.020	[0.013, 0.030]	[0.0088, 0.046]
3.00	0.0084	0.013	[0.0088, 0.020]	[0.0061, 0.031]
3.50	0.0091	0.011	[0.0073, 0.017]	[0.0051, 0.025]
4.00	0.0092	0.010	[0.0064, 0.015]	[0.0044, 0.023]
4.50	0.0087	0.010	[0.0067, 0.016]	[0.0046, 0.024]
5.00	0.0097	0.012	[0.0078, 0.019]	[0.0056, 0.029]
6.00	0.015	0.021	[0.014, 0.034]	[0.0095, 0.053]
6.50	0.016	0.025	[0.017, 0.040]	[0.011, 0.062]
7.00	0.022	0.032	[0.021, 0.050]	[0.014, 0.081]

Table 4: Limits at 95% CL on the product of the resonance production cross section and branching fraction for the extra-wide ($\Gamma/m = 30\%$) Z' boson resonance hypothesis.

Mass [TeV]	Obs. [pb]	Median exp. [pb]	68% Exp. [pb]	95% Exp. [pb]
1.0	2.0	1.1	[0.63, 1.8]	[0.41, 2.7]
2.0	0.078	0.066	[0.041, 0.11]	[0.027, 0.18]
3.0	0.019	0.026	[0.017, 0.040]	[0.012, 0.061]
4.0	0.019	0.023	[0.015, 0.035]	[0.011, 0.053]
5.0	0.022	0.025	[0.016, 0.039]	[0.011, 0.062]
6.0	0.029	0.035	[0.023, 0.055]	[0.015, 0.086]
6.5	0.030	0.040	[0.026, 0.061]	[0.018, 0.097]
7.0	0.035	0.044	[0.029, 0.070]	[0.019, 0.11]

Table 5: Limits at 95% CL on the product of the resonance production cross section and branching fraction for the g_{KK} gluon resonance hypothesis.

Mass [TeV]	Obs. [pb]	Median exp. [pb]	68% Exp. [pb]	95% Exp. [pb]
0.50	9.5	30	[13, 55]	[6.1, 82]
0.75	4.6	5.0	[2.6, 8.3]	[1.5, 13]
1.00	0.71	0.99	[0.64, 1.5]	[0.44, 2.3]
1.25	0.77	0.42	[0.26, 0.67]	[0.18, 1.0]
1.50	0.30	0.19	[0.12, 0.32]	[0.081, 0.56]
2.00	0.090	0.065	[0.042, 0.10]	[0.028, 0.17]
2.50	0.045	0.035	[0.022, 0.055]	[0.015, 0.089]
3.00	0.021	0.025	[0.017, 0.039]	[0.012, 0.061]
3.50	0.016	0.022	[0.014, 0.033]	[0.0098, 0.051]
4.00	0.020	0.021	[0.014, 0.032]	[0.0096, 0.050]
4.50	0.019	0.024	[0.016, 0.038]	[0.011, 0.059]
5.00	0.025	0.030	[0.020, 0.047]	[0.014, 0.074]

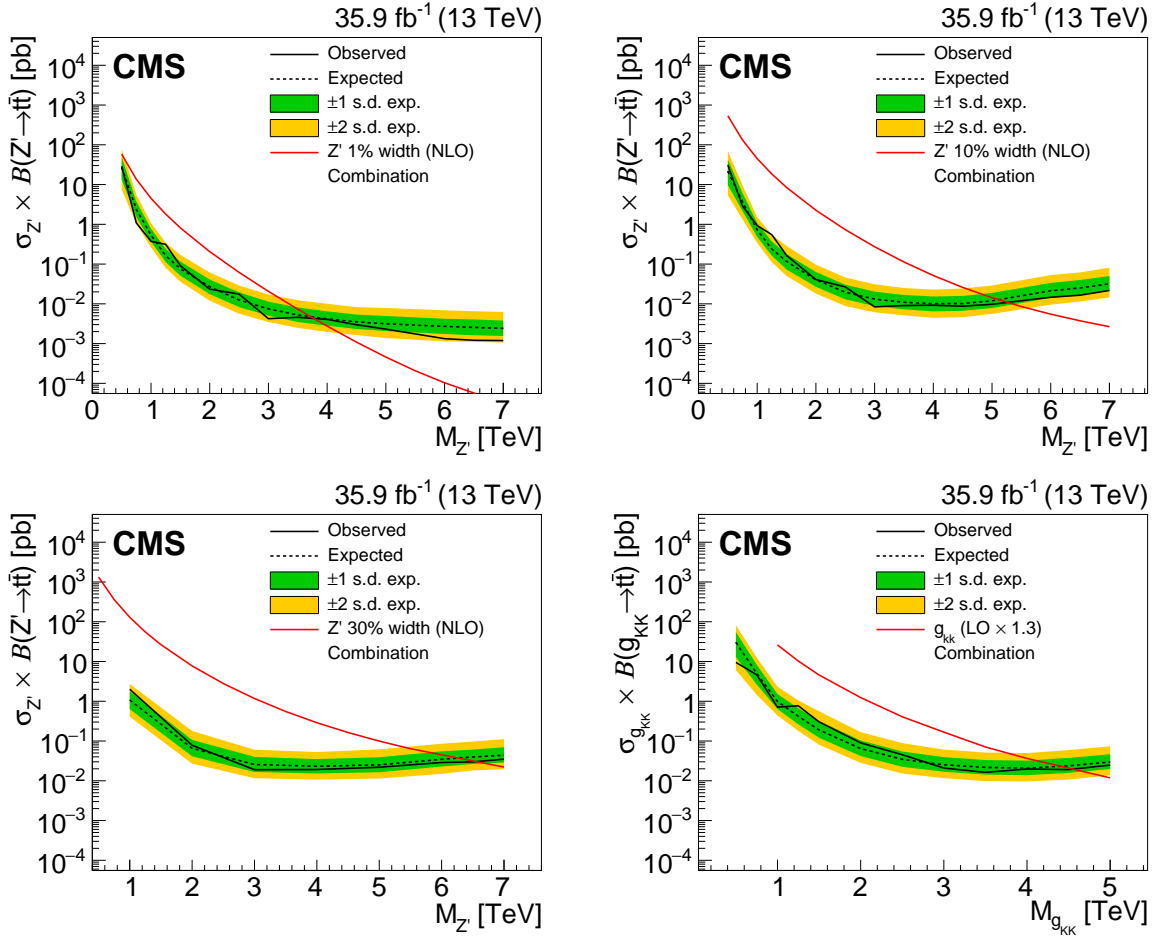


Figure 13: Observed and expected limits at 95% CL for each of the four signal hypotheses considered in this analysis.

wide Z' bosons with masses up to 6.65 TeV (6.40 TeV expected). For the g_{KK} resonance hypothesis, the analysis excludes masses up to 4.55 TeV (4.45 TeV expected). These results represent a significant improvement on the previous results in this channel from the 2015 data taking period, not only because of the increase in integrated luminosity, but also the reduction in the uncertainty in the multijet background estimate in the fully hadronic channel, the improved W +jets rejection via the W +jets BDT in the single-lepton channel, and the inclusion of dilepton event categories in the combination. The absolute cross section limits are 10–40% better, for $m_{t\bar{t}}$ above 2 TeV, than the previous result released by CMS [31] scaled to an integrated luminosity of 35.9 fb^{-1} . These results are the most stringent exclusion limits on a $t\bar{t}$ resonance to date.

11 Summary

A search for a generic massive top quark and antiquark ($t\bar{t}$) resonance has been presented. The analysis was performed using data collected by the CMS experiment in 2016 at the LHC at $\sqrt{s} = 13 \text{ TeV}$, corresponding to an integrated luminosity of 35.9 fb^{-1} . The analysis is focused on searching for a $t\bar{t}$ resonance above 2 TeV, where the decay products of the top quark become collimated because of its large Lorentz boost. The analysis performed a simultaneous measurement of the backgrounds and the t tagging efficiency from data. The data are consistent with the background-only hypothesis, and no evidence for a massive $t\bar{t}$ resonance has been found.

Limits at 95% confidence level are calculated for the production cross section for a spin-1 resonance decaying to $t\bar{t}$ pairs with a variety of decay widths.

Limits were calculated for two benchmark signal processes that decay to $t\bar{t}$ pairs. A topcolor Z' boson with relative widths of 1, 10, or 30% is excluded in the mass ranges 0.50–3.80, 0.50–5.25, and 0.50–6.65 TeV, respectively. The first Kaluza–Klein excitation of the gluon in the Randall–Sundrum scenario (g_{KK}) is excluded in the range 0.50–4.55 TeV. This is the first search by any experiment at $\sqrt{s} = 13$ TeV for $t\bar{t}$ resonances that combines all three decay topologies of the $t\bar{t}$ system: dilepton, single-lepton, and fully hadronic.

The sensitivity of the analysis exceeds previous searches at $\sqrt{s} = 8$ and 13 TeV, particularly at high $t\bar{t}$ invariant mass. Previous measurements have excluded a topcolor Z' up to 3.0, 3.9, and 4.0 TeV, for relative widths of 1, 10, and 30%, and g_{KK} from 3.3 to 3.8 TeV, depending on model [31, 32]. The presented analysis improves upon those limits, extending the Z' exclusions to 3.80, 5.25, and 6.65 TeV and the g_{KK} exclusion to 4.55 TeV. These are the most stringent limits on the topcolor Z' and g_{KK} models to date.

Acknowledgments

We congratulate our colleagues in the CERN accelerator departments for the excellent performance of the LHC and thank the technical and administrative staffs at CERN and at other CMS institutes for their contributions to the success of the CMS effort. In addition, we gratefully acknowledge the computing centers and personnel of the Worldwide LHC Computing Grid for delivering so effectively the computing infrastructure essential to our analyses. Finally, we acknowledge the enduring support for the construction and operation of the LHC and the CMS detector provided by the following funding agencies: BMBWF and FWF (Austria); FNRS and FWO (Belgium); CNPq, CAPES, FAPERJ, FAPERGS, and FAPESP (Brazil); MES (Bulgaria); CERN; CAS, MoST, and NSFC (China); COLCIENCIAS (Colombia); MSES and CSF (Croatia); RPF (Cyprus); SENESCYT (Ecuador); MoER, ERC IUT, and ERDF (Estonia); Academy of Finland, MEC, and HIP (Finland); CEA and CNRS/IN2P3 (France); BMBF, DFG, and HGF (Germany); GSRT (Greece); NKFIA (Hungary); DAE and DST (India); IPM (Iran); SFI (Ireland); INFN (Italy); MSIP and NRF (Republic of Korea); MES (Latvia); LAS (Lithuania); MOE and UM (Malaysia); BUAP, CINVESTAV, CONACYT, LNS, SEP, and UASLP-FAI (Mexico); MOS (Montenegro); MBIE (New Zealand); PAEC (Pakistan); MSHE and NSC (Poland); FCT (Portugal); JINR (Dubna); MON, RosAtom, RAS, RFBR, and NRC KI (Russia); MESTD (Serbia); SEIDI, CPAN, PCTI, and FEDER (Spain); MOSTR (Sri Lanka); Swiss Funding Agencies (Switzerland); MST (Taipei); ThEPCenter, IPST, STAR, and NSTDA (Thailand); TUBITAK and TAEK (Turkey); NASU and SFFR (Ukraine); STFC (United Kingdom); DOE and NSF (USA).

Individuals have received support from the Marie-Curie program and the European Research Council and Horizon 2020 Grant, contract No. 675440 (European Union); the Leventis Foundation; the A. P. Sloan Foundation; the Alexander von Humboldt Foundation; the Belgian Federal Science Policy Office; the Fonds pour la Formation à la Recherche dans l'Industrie et dans l'Agriculture (FRIA-Belgium); the Agentschap voor Innovatie door Wetenschap en Technologie (IWT-Belgium); the F.R.S.-FNRS and FWO (Belgium) under the “Excellence of Science - EOS” - be.h project n. 30820817; the Ministry of Education, Youth and Sports (MEYS) of the Czech Republic; the Lendület (“Momentum”) Program and the János Bolyai Research Scholarship of the Hungarian Academy of Sciences, the New National Excellence Program ÚNKP, the NKFIA research grants 123842, 123959, 124845, 124850 and 125105 (Hungary); the Council of Science and Industrial Research, India; the HOMING PLUS program of the Foundation for Polish Science, cofinanced from European Union, Regional Development Fund, the Mobility Plus program of

the Ministry of Science and Higher Education, the National Science Center (Poland), contracts Harmonia 2014/14/M/ST2/00428, Opus 2014/13/B/ST2/02543, 2014/15/B/ST2/03998, and 2015/19/B/ST2/02861, Sonata-bis 2012/07/E/ST2/01406; the National Priorities Research Program by Qatar National Research Fund; the Programa Estatal de Fomento de la Investigación Científica y Técnica de Excelencia María de Maeztu, grant MDM-2015-0509 and the Programa Severo Ochoa del Principado de Asturias; the Thalís and Aristeia programs cofinanced by EU-ESF and the Greek NSRF; the Rachadapisek Sompot Fund for Postdoctoral Fellowship, Chulalongkorn University and the Chulalongkorn Academic into Its 2nd Century Project Advancement Project (Thailand); the Welch Foundation, contract C-1845; and the Weston Havens Foundation (USA).

References

- [1] CDF Collaboration, "Observation of top quark production in $p\bar{p}$ collisions", *Phys. Rev. Lett.* **74** (1995) 2626, doi:10.1103/PhysRevLett.74.2626, arXiv:hep-ex/9503002.
- [2] D0 Collaboration, "Observation of the top quark", *Phys. Rev. Lett.* **74** (1995) 2632, doi:10.1103/PhysRevLett.74.2632, arXiv:hep-ex/9503003.
- [3] J. L. Rosner, "Prominent decay modes of a leptophobic Z' ", *Phys. Lett. B* **387** (1996) 113, doi:10.1016/0370-2693(96)01022-2, arXiv:hep-ph/9607207.
- [4] K. R. Lynch, S. Mrenna, M. Narain, and E. H. Simmons, "Finding Z' bosons coupled preferentially to the third family at CERN LEP and the Fermilab Tevatron", *Phys. Rev. D* **63** (2001) 035006, doi:10.1103/PhysRevD.63.035006, arXiv:hep-ph/0007286.
- [5] M. Carena, A. Daleo, B. A. Dobrescu, and T. M. P. Tait, " Z' gauge bosons at the Fermilab Tevatron", *Phys. Rev. D* **70** (2004) 093009, doi:10.1103/PhysRevD.70.093009, arXiv:hep-ph/0408098.
- [6] D. Dicus, A. Stange, and S. Willenbrock, "Higgs decay to top quarks at hadron colliders", *Phys. Lett. B* **333** (1994) 126, doi:10.1016/0370-2693(94)91017-0, arXiv:hep-ph/9404359.
- [7] P. H. Frampton and S. L. Glashow, "Chiral color: an alternative to the standard model", *Phys. Lett. B* **190** (1987) 157, doi:10.1016/0370-2693(87)90859-8.
- [8] D. Choudhury, R. M. Godbole, R. K. Singh, and K. Wagh, "Top production at the Tevatron/LHC and nonstandard, strongly interacting spin one particles", *Phys. Lett. B* **657** (2007) 69, doi:10.1016/j.physletb.2007.09.057, arXiv:0705.1499. Updates in arXiv:0810.3635.
- [9] R. M. Godbole and D. Choudhury, "Nonstandard, strongly interacting spin one $t\bar{t}$ resonances", in *Proceedings, 34th international conference on high energy physics (ICHEP 2008): Philadelphia, Pennsylvania, July 30-August 5, 2008*. arXiv:0810.3635.
- [10] C. T. Hill, "Topcolor: top quark condensation in a gauge extension of the standard model", *Phys. Lett. B* **266** (1991) 419, doi:10.1016/0370-2693(91)91061-Y.
- [11] C. T. Hill and S. J. Parke, "Top production: sensitivity to new physics", *Phys. Rev. D* **49** (1994) 4454, doi:10.1103/PhysRevD.49.4454, arXiv:hep-ph/9312324.
- [12] C. T. Hill, "Topcolor assisted technicolor", *Phys. Lett. B* **345** (1995) 483, doi:10.1016/0370-2693(94)01660-5, arXiv:hep-ph/9411426. Updates in arXiv:hep-ph/9911288.
- [13] R. M. Harris, C. T. Hill, and S. J. Parke, "Cross section for topcolor Z'_t decaying to $t\bar{t}$ ", (1999). arXiv:hep-ph/9911288.
- [14] R. M. Harris and S. Jain, "Cross sections for leptophobic topcolor Z' decaying to top-antitop", *Eur. Phys. J. C* **72** (2012) 2072, doi:10.1140/epjc/s10052-012-2072-4, arXiv:1112.4928.
- [15] L. Randall and R. Sundrum, "A large mass hierarchy from a small extra dimension", *Phys. Rev. Lett.* **83** (1999) 3370, doi:10.1103/PhysRevLett.83.3370, arXiv:hep-ph/9905221.

-
- [16] L. Randall and R. Sundrum, "An alternative to compactification", *Phys. Rev. Lett.* **83** (1999) 4690, doi:10.1103/PhysRevLett.83.4690, arXiv:hep-th/9906064.
- [17] K. Agashe et al., "LHC signals from warped extra dimensions", *Phys. Rev. D* **77** (2008) 015003, doi:10.1103/PhysRevD.77.015003, arXiv:hep-ph/0612015.
- [18] H. Davoudiasl, J. L. Hewett, and T. G. Rizzo, "Phenomenology of the Randall-Sundrum gauge hierarchy model", *Phys. Rev. Lett.* **84** (2000) 2080, doi:10.1103/PhysRevLett.84.2080, arXiv:hep-ph/9909255.
- [19] CDF Collaboration, "Limits on the production of narrow $t\bar{t}$ resonances in $p\bar{p}$ collisions at $\sqrt{s} = 1.96$ TeV", *Phys. Rev. D* **77** (2008) 051102, doi:10.1103/PhysRevD.77.051102, arXiv:0710.5335.
- [20] CDF Collaboration, "Search for resonant $t\bar{t}$ production in $p\bar{p}$ collisions at $\sqrt{s} = 1.96$ TeV", *Phys. Rev. Lett.* **100** (2008) 231801, doi:10.1103/PhysRevLett.100.231801, arXiv:0709.0705.
- [21] CDF Collaboration, "A search for resonant production of $t\bar{t}$ pairs in 4.8 fb^{-1} of integrated luminosity of $p\bar{p}$ collisions at $\sqrt{s} = 1.96$ TeV", *Phys. Rev. D* **84** (2011) 072004, doi:10.1103/PhysRevD.84.072004, arXiv:1107.5063.
- [22] D0 Collaboration, "Search for a narrow $t\bar{t}$ resonance in $p\bar{p}$ collisions at $\sqrt{s} = 1.96$ TeV", *Phys. Rev. D* **85** (2012) 051101, doi:10.1103/PhysRevD.85.051101, arXiv:1111.1271.
- [23] CDF Collaboration, "Search for resonant production of $t\bar{t}$ decaying to jets in $p\bar{p}$ collisions at $\sqrt{s} = 1.96$ TeV", *Phys. Rev. D* **84** (2011) 072003, doi:10.1103/PhysRevD.84.072003, arXiv:1108.4755.
- [24] D0 Collaboration, "Search for $t\bar{t}$ resonances in the lepton plus jets final state in $p\bar{p}$ collisions at $\sqrt{s} = 1.96$ TeV", *Phys. Lett. B* **668** (2008) 98, doi:10.1016/j.physletb.2008.08.027, arXiv:0804.3664.
- [25] CMS Collaboration, "Search for anomalous $t\bar{t}$ production in the highly-boosted all-hadronic final state", *JHEP* **09** (2012) 029, doi:10.1007/JHEP09(2012)029, arXiv:1204.2488. [Erratum: doi:10.1007/JHEP03(2014)132].
- [26] ATLAS Collaboration, "A search for $t\bar{t}$ resonances in lepton+jets events with highly boosted top quarks collected in pp collisions at $\sqrt{s} = 7$ TeV with the ATLAS detector", *JHEP* **09** (2012) 041, doi:10.1007/JHEP09(2012)041, arXiv:1207.2409.
- [27] ATLAS Collaboration, "Search for $t\bar{t}$ resonances in the lepton plus jets final state with ATLAS using 4.7 fb^{-1} of pp collisions at $\sqrt{s} = 7$ TeV", *Phys. Rev. D* **88** (2013) 012004, doi:10.1103/PhysRevD.88.012004, arXiv:1305.2756.
- [28] CMS Collaboration, "Search for resonant $t\bar{t}$ production in lepton+jets events in pp collisions at $\sqrt{s} = 7$ TeV", *JHEP* **12** (2012) 015, doi:10.1007/JHEP12(2012)015, arXiv:1209.4397.
- [29] CMS Collaboration, "Search for Z' resonances decaying to $t\bar{t}$ in dilepton+jets final states in pp collisions at $\sqrt{s} = 7$ TeV", *Phys. Rev. D* **87** (2013) 072002, doi:10.1103/PhysRevD.87.072002, arXiv:1211.3338.

- [30] CMS Collaboration, “Searches for new physics using the $t\bar{t}$ invariant mass distribution in pp collisions at $\sqrt{s} = 8$ TeV”, *Phys. Rev. Lett.* **111** (2013) 211804, doi:10.1103/PhysRevLett.111.211804, arXiv:1309.2030. [Erratum: doi:10.1103/PhysRevLett(2014)112].
- [31] CMS Collaboration, “Search for $t\bar{t}$ resonances in highly boosted lepton+jets and fully hadronic final states in proton-proton collisions at $\sqrt{s} = 13$ TeV”, *JHEP* **07** (2017) 001, doi:10.1007/JHEP07(2017)001, arXiv:1704.03366.
- [32] ATLAS Collaboration, “Search for heavy particles decaying into top-quark pairs using lepton-plus-jets events in proton-proton collisions at $\sqrt{s} = 13$ TeV with the ATLAS detector”, *Eur. Phys. J. C* **78** (2018) 565, doi:10.1140/epjc/s10052-018-5995-6, arXiv:1804.10823.
- [33] CMS Collaboration, “Identification of heavy-flavour jets with the CMS detector in pp collisions at 13 TeV”, *JINST* **13** (2018) P05011, doi:10.1088/1748-0221/13/05/P05011, arXiv:1712.07158.
- [34] CMS Collaboration, “The CMS trigger system”, *JINST* **12** (2017) P01020, doi:10.1088/1748-0221/12/01/P01020, arXiv:1609.02366.
- [35] CMS Collaboration, “The CMS experiment at the CERN LHC”, *JINST* **3** (2008) S08004, doi:10.1088/1748-0221/3/08/S08004.
- [36] CMS Collaboration, “Particle-flow reconstruction and global event description with the CMS detector”, *JINST* **12** (2017) P10003, doi:10.1088/1748-0221/12/10/P10003, arXiv:1706.04965.
- [37] CMS Collaboration, “Description and performance of track and primary-vertex reconstruction with the CMS tracker”, *JINST* **9** (2014) P10009, doi:10.1088/1748-0221/9/10/P10009, arXiv:1405.6569.
- [38] M. Cacciari, G. P. Salam, and G. Soyez, “The anti- k_T jet clustering algorithm”, *JHEP* **04** (2008) 063, doi:10.1088/1126-6708/2008/04/063, arXiv:0802.1189.
- [39] M. Cacciari, G. P. Salam, and G. Soyez, “FastJet user manual”, *Eur. Phys. J. C* **72** (2012) 1896, doi:10.1140/epjc/s10052-012-1896-2, arXiv:1111.6097.
- [40] CMS Collaboration, “Determination of jet energy calibration and transverse momentum resolution in CMS”, *JINST* **6** (2011) P11002, doi:10.1088/1748-0221/6/11/P11002, arXiv:1107.4277.
- [41] CMS Collaboration, “Performance of electron reconstruction and selection with the CMS detector in proton-proton collisions at $\sqrt{s} = 8$ TeV”, *JINST* **10** (2015) P06005, doi:10.1088/1748-0221/10/06/P06005, arXiv:1502.02701.
- [42] CMS Collaboration, “Energy calibration and resolution of the CMS electromagnetic calorimeter in pp collisions at $\sqrt{s} = 7$ TeV”, *JINST* **8** (2013) P09009, doi:10.1088/1748-0221/8/09/P09009, arXiv:1306.2016.
- [43] M. Cacciari, G. P. Salam, and G. Soyez, “The catchment area of jets”, *JHEP* **04** (2008) 005, doi:10.1088/1126-6708/2008/04/005, arXiv:0802.1188.
- [44] CMS Collaboration, “Top tagging with new approaches”, CMS Physics Analysis Summary CMS-PAS-JME-15-002, 2016.

-
- [45] CMS Collaboration, “Jet performance in pp collisions at 7 TeV”, CMS Physics Analysis Summary CMS-PAS-JME-10-003, 2010.
- [46] CMS Collaboration, “Missing transverse energy performance of the CMS detector”, *JINST* **6** (2011) P09001, doi:10.1088/1748-0221/6/09/P09001, arXiv:1106.5048.
- [47] CMS Collaboration, “A Cambridge-Aachen (C-A) based jet algorithm for boosted top-jet tagging”, CMS Physics Analysis Summary CMS-PAS-JME-09-001, 2009.
- [48] CMS Collaboration, “Boosted top-jet tagging at CMS”, CMS Physics Analysis Summary CMS-PAS-JME-13-007, 2014.
- [49] D. E. Kaplan, K. Rehermann, M. D. Schwartz, and B. Tweedie, “Top tagging: a method for identifying boosted hadronically decaying top quarks”, *Phys. Rev. Lett.* **101** (2008) 142001, doi:10.1103/PhysRevLett.101.142001, arXiv:0806.0848.
- [50] D. Bertolini, P. Harris, M. Low, and N. Tran, “Pileup per particle identification”, *JHEP* **10** (2014) 059, doi:10.1007/JHEP10(2014)059, arXiv:1407.6013.
- [51] Y. L. Dokshitzer, G. D. Leder, S. Moretti, and B. R. Webber, “Better jet clustering algorithms”, *JHEP* **08** (1997) 001, doi:10.1088/1126-6708/1997/08/001, arXiv:hep-ph/9707323.
- [52] M. Dasgupta, A. Fregoso, S. Marzani, and G. P. Salam, “Towards an understanding of jet substructure”, *JHEP* **09** (2013) 029, doi:10.1007/JHEP09(2013)029, arXiv:1307.0007.
- [53] A. J. Larkoski, S. Marzani, G. Soyez, and J. Thaler, “Soft drop”, *JHEP* **05** (2014) 146, doi:10.1007/JHEP05(2014)146, arXiv:1402.2657.
- [54] J. Thaler and K. Van Tilburg, “Identifying boosted objects with n -subjettiness”, *JHEP* **03** (2011) 015, doi:10.1007/JHEP03(2011)015, arXiv:1011.2268.
- [55] J. Thaler and K. Van Tilburg, “Maximizing boosted top identification by minimizing n -subjettiness”, *JHEP* **02** (2012) 093, doi:10.1007/JHEP02(2012)093, arXiv:1108.2701.
- [56] J. Alwall et al., “The automated computation of tree-level and next-to-leading order differential cross sections, and their matching to parton shower simulations”, *JHEP* **07** (2014) 079, doi:10.1007/JHEP07(2014)079, arXiv:1405.0301.
- [57] J. Alwall et al., “Comparative study of various algorithms for the merging of parton showers and matrix elements in hadronic collisions”, *Eur. Phys. J. C* **53** (2008) 473, doi:10.1140/epjc/s10052-007-0490-5, arXiv:0706.2569.
- [58] T. Sjöstrand et al., “An introduction to PYTHIA 8.2”, *Comput. Phys. Commun.* **191** (2015) 159, doi:10.1016/j.cpc.2015.01.024, arXiv:1410.3012.
- [59] S. Ask et al., “Identifying the colour of TeV-scale resonances”, *JHEP* **01** (2012) 018, doi:10.1007/JHEP01(2012)018, arXiv:1108.2396.
- [60] R. Bonciani et al., “Electroweak top-quark pair production at the LHC with Z' bosons to NLO QCD in POWHEG”, *JHEP* **02** (2016) 141, doi:10.1007/JHEP02(2016)141, arXiv:1511.08185.

- [61] P. Nason, “A new method for combining NLO QCD with shower Monte Carlo algorithms”, *JHEP* **11** (2004) 040, doi:10.1088/1126-6708/2004/11/040, arXiv:hep-ph/0409146.
- [62] S. Frixione, P. Nason, and G. Ridolfi, “A positive-weight next-to-leading-order Monte Carlo for heavy flavour hadroproduction”, *JHEP* **09** (2007) 126, doi:10.1088/1126-6708/2007/09/126, arXiv:0707.3088.
- [63] S. Frixione, P. Nason, and C. Oleari, “Matching NLO QCD computations with parton shower simulations: the POWHEG method”, *JHEP* **11** (2007) 070, doi:10.1088/1126-6708/2007/11/070, arXiv:0709.2092.
- [64] S. Alioli, P. Nason, C. Oleari, and E. Re, “A general framework for implementing NLO calculations in shower Monte Carlo programs: the POWHEG BOX”, *JHEP* **06** (2010) 043, doi:10.1007/JHEP06(2010)043, arXiv:1002.2581.
- [65] S. Alioli, P. Nason, C. Oleari, and E. Re, “NLO single-top production matched with shower in POWHEG: s - and t -channel contributions”, *JHEP* **09** (2009) 111, doi:10.1088/1126-6708/2009/09/111, arXiv:0907.4076. [Erratum: doi:10.1007/JHEP02(2010)011].
- [66] E. Re, “Single-top Wt -channel production matched with parton showers using the POWHEG method”, *Eur. Phys. J. C* **71** (2011) 1547, doi:10.1140/epjc/s10052-011-1547-z, arXiv:1009.2450.
- [67] R. Frederix and S. Frixione, “Merging meets matching in MC@NLO”, *JHEP* **12** (2012) 061, doi:10.1007/JHEP12(2012)061, arXiv:1209.6215.
- [68] CMS Collaboration, “Event generator tunes obtained from underlying event and multiparton scattering measurements”, *Eur. Phys. J. C* **76** (2016) 155, doi:10.1140/epjc/s10052-016-3988-x, arXiv:1512.00815.
- [69] NNPDF Collaboration, “Parton distributions for the LHC run II”, *JHEP* **04** (2015) 040, doi:10.1007/JHEP04(2015)040, arXiv:1410.8849.
- [70] M. Czakon and A. Mitov, “Top++: a program for the calculation of the top-pair cross-section at hadron colliders”, *Comput. Phys. Commun.* **185** (2014) 2930, doi:10.1016/j.cpc.2014.06.021, arXiv:1112.5675.
- [71] Y. Li and F. Petriello, “Combining QCD and electroweak corrections to dilepton production in FEWZ”, *Phys. Rev. D* **86** (2012) 094034, doi:10.1103/PhysRevD.86.094034, arXiv:1208.5967.
- [72] P. Kant et al., “HatHor for single top-quark production: updated predictions and uncertainty estimates for single top-quark production in hadronic collisions”, *Comput. Phys. Commun.* **191** (2015) 74, doi:10.1016/j.cpc.2015.02.001, arXiv:1406.4403.
- [73] N. Kidonakis, “NNLL threshold resummation for top-pair and single-top production”, *Phys. Part. Nucl.* **45** (2014) 714, doi:10.1134/S1063779614040091, arXiv:1210.7813.
- [74] GEANT4 Collaboration, “GEANT4 — a simulation toolkit”, *Nucl. Instrum. Meth. A* **506** (2003) 250, doi:10.1016/S0168-9002(03)01368-8.

- [75] M. Hildreth, V. N. Ivanchenko, D. J. Lange, and M. J. Kortelainen, “CMS full simulation for run-2”, *J. Phys. Conf. Ser.* **664** (2015) 072022, doi:10.1088/1742-6596/664/7/072022.
- [76] B. P. Roe et al., “Boosted decision trees, an alternative to artificial neural networks”, *Nucl. Instrum. Meth. A* **543** (2005) 577, doi:10.1016/j.nima.2004.12.018, arXiv:physics/0408124.
- [77] H. Voss, A. Höcker, J. Stelzer, and F. Tegenfeldt, “TMVA, the toolkit for multivariate data analysis with ROOT”, in *XIth International Workshop on Advanced Computing and Analysis Techniques in Physics Research (ACAT)*, p. 40. 2007. arXiv:physics/0703039. doi:10.22323/1.050.0040.
- [78] J. D. Bjorken and S. J. Brodsky, “Statistical model for electron-positron annihilation into hadrons”, *Phys. Rev. D* **1** (1970) 1416, doi:10.1103/PhysRevD.1.1416.
- [79] G. Hanson et al., “Evidence for jet structure in hadron production by $e^+ e^-$ annihilation”, *Phys. Rev. Lett.* **35** (1975) 1609, doi:10.1103/PhysRevLett.35.1609.
- [80] CMS Collaboration, “CMS luminosity measurement for the 2016 data taking period”, CMS Physics Analysis Summary CMS-PAS-LUM-17-001, CERN, 2017.
- [81] CMS Collaboration, “Measurement of the inelastic proton-proton cross section at $\sqrt{s} = 13$ TeV”, (2018). arXiv:1802.02613.
- [82] ATLAS Collaboration, “Measurement of the inelastic proton-proton cross section at $\sqrt{s} = 13$ TeV with the ATLAS detector at the LHC”, *Phys. Rev. Lett.* **117** (2016) 182002, doi:10.1103/PhysRevLett.117.182002, arXiv:1606.02625.
- [83] J. Butterworth et al., “PDF4LHC recommendations for LHC run II”, *J. Phys. G* **43** (2016) 023001, doi:10.1088/0954-3899/43/2/023001, arXiv:1510.03865.
- [84] CMS Collaboration, “Measurement of differential cross sections for top quark pair production using the lepton+jets final state in proton-proton collisions at 13 TeV”, *Phys. Rev. D* **95** (2017) 092001, doi:10.1103/PhysRevD.95.092001, arXiv:1610.04191.
- [85] J. Ott, “THETA — A framework for template-based modeling and inference”, 2010. <http://www-ekp.physik.uni-karlsruhe.de/~ott/theta/theta-auto>.
- [86] G. Cowan, “Statistics”, Ch. 39 in Particle Data Group, “Review of particle physics”, *Chin. Phys. C* **40** (2016) 100001, doi:10.1088/1674-1137/40/10/100001.
- [87] ATLAS and CMS Collaborations, The LHC Higgs Combination Group, “Procedure for the LHC Higgs boson search combination in summer 2011”, Technical Report CMS-NOTE-2011-005. ATL-PHYS-PUB-2011-11, 2011.
- [88] R. J. Barlow and C. Beeston, “Fitting using finite Monte Carlo samples”, *Comput. Phys. Commun.* **77** (1993) 219, doi:10.1016/0010-4655(93)90005-w.

A The CMS Collaboration

Yerevan Physics Institute, Yerevan, Armenia

A.M. Sirunyan, A. Tumasyan

Institut für Hochenergiephysik, Wien, Austria

W. Adam, F. Ambrogi, E. Asilar, T. Bergauer, J. Brandstetter, M. Dragicevic, J. Erö, A. Escalante Del Valle, M. Flechl, R. Frühwirth¹, V.M. Ghete, J. Hrubec, M. Jeitler¹, N. Krammer, I. Krätschmer, D. Liko, T. Madlener, I. Mikulec, N. Rad, H. Rohringer, J. Schieck¹, R. Schöfbeck, M. Spanring, D. Spitzbart, A. Taurok, W. Waltenberger, J. Wittmann, C.-E. Wulz¹, M. Zarucki

Institute for Nuclear Problems, Minsk, Belarus

V. Chekhovsky, V. Mossolov, J. Suarez Gonzalez

Universiteit Antwerpen, Antwerpen, Belgium

E.A. De Wolf, D. Di Croce, X. Janssen, J. Lauwers, M. Pieters, H. Van Haeve, P. Van Mechelen, N. Van Remortel

Vrije Universiteit Brussel, Brussel, Belgium

S. Abu Zeid, F. Blekman, J. D'Hondt, I. De Bruyn, J. De Clercq, K. Deroover, G. Flouris, D. Lontkovskyi, S. Lowette, I. Marchesini, S. Moortgat, L. Moreels, Q. Python, K. Skovpen, S. Tavernier, W. Van Doninck, P. Van Mulders, I. Van Parijs

Université Libre de Bruxelles, Bruxelles, Belgium

D. Beghin, B. Bilin, H. Brun, B. Clerbaux, G. De Lentdecker, H. Delannoy, B. Dorney, G. Fasanella, L. Favart, R. Goldouzian, A. Grebenyuk, A.K. Kalsi, T. Lenzi, J. Luetic, N. Postiau, E. Starling, L. Thomas, C. Vander Velde, P. Vanlaer, D. Vannerom, Q. Wang

Ghent University, Ghent, Belgium

T. Cornelis, D. Dobur, A. Fagot, M. Gul, I. Khvastunov², D. Poyraz, C. Roskas, D. Trocino, M. Tytgat, W. Verbeke, B. Vermassen, M. Vit, N. Zaganidis

Université Catholique de Louvain, Louvain-la-Neuve, Belgium

H. Bakhshiansohi, O. Bondu, S. Brochet, G. Bruno, C. Caputo, P. David, C. Delaere, M. Delcourt, A. Giammanco, G. Krintiras, V. Lemaître, A. Magitteri, A. Mertens, M. Musich, K. Piotrkowski, A. Saggio, M. Vidal Marono, S. Wertz, J. Zobec

Centro Brasileiro de Pesquisas Físicas, Rio de Janeiro, Brazil

F.L. Alves, G.A. Alves, M. Correa Martins Junior, G. Correia Silva, C. Hensel, A. Moraes, M.E. Pol, P. Rebello Teles

Universidade do Estado do Rio de Janeiro, Rio de Janeiro, Brazil

E. Belchior Batista Das Chagas, W. Carvalho, J. Chinellato³, E. Coelho, E.M. Da Costa, G.G. Da Silveira⁴, D. De Jesus Damiao, C. De Oliveira Martins, S. Fonseca De Souza, H. Malbouisson, D. Matos Figueiredo, M. Melo De Almeida, C. Mora Herrera, L. Mundim, H. Nogima, W.L. Prado Da Silva, L.J. Sanchez Rosas, A. Santoro, A. Sznajder, M. Thiel, E.J. Tonelli Manganote³, F. Torres Da Silva De Araujo, A. Vilela Pereira

Universidade Estadual Paulista ^a, Universidade Federal do ABC ^b, São Paulo, Brazil

S. Ahuja^a, C.A. Bernardes^a, L. Calligaris^a, T.R. Fernandez Perez Tomei^a, E.M. Gregores^b, P.G. Mercadante^b, S.F. Novaes^a, SandraS. Padula^a

Institute for Nuclear Research and Nuclear Energy, Bulgarian Academy of Sciences, Sofia,

Bulgaria

A. Aleksandrov, R. Hadjiiska, P. Iaydjiev, A. Marinov, M. Misheva, M. Rodozov, M. Shopova, G. Sultanov

University of Sofia, Sofia, Bulgaria

A. Dimitrov, L. Litov, B. Pavlov, P. Petkov

Beihang University, Beijing, China

W. Fang⁵, X. Gao⁵, L. Yuan

Institute of High Energy Physics, Beijing, China

M. Ahmad, J.G. Bian, G.M. Chen, H.S. Chen, M. Chen, Y. Chen, C.H. Jiang, D. Leggat, H. Liao, Z. Liu, F. Romeo, S.M. Shaheen⁶, A. Spiezia, J. Tao, Z. Wang, E. Yazgan, H. Zhang, S. Zhang⁶, J. Zhao

State Key Laboratory of Nuclear Physics and Technology, Peking University, Beijing, China

Y. Ban, G. Chen, A. Levin, J. Li, L. Li, Q. Li, Y. Mao, S.J. Qian, D. Wang, Z. Xu

Tsinghua University, Beijing, China

Y. Wang

Universidad de Los Andes, Bogota, Colombia

C. Avila, A. Cabrera, C.A. Carrillo Montoya, L.F. Chaparro Sierra, C. Florez, C.F. González Hernández, M.A. Segura Delgado

University of Split, Faculty of Electrical Engineering, Mechanical Engineering and Naval Architecture, Split, Croatia

B. Courbon, N. Godinovic, D. Lelas, I. Puljak, T. Sculac

University of Split, Faculty of Science, Split, Croatia

Z. Antunovic, M. Kovac

Institute Rudjer Boskovic, Zagreb, Croatia

V. Brigljevic, D. Ferencek, K. Kadija, B. Mesic, A. Starodumov⁷, T. Susa

University of Cyprus, Nicosia, Cyprus

M.W. Ather, A. Attikis, M. Kolosova, G. Mavromanolakis, J. Mousa, C. Nicolaou, F. Ptochos, P.A. Razis, H. Rykaczewski

Charles University, Prague, Czech Republic

M. Finger⁸, M. Finger Jr.⁸

Escuela Politecnica Nacional, Quito, Ecuador

E. Ayala

Universidad San Francisco de Quito, Quito, Ecuador

E. Carrera Jarrin

Academy of Scientific Research and Technology of the Arab Republic of Egypt, Egyptian Network of High Energy Physics, Cairo, Egypt

A. Mahrous⁹, A. Mohamed¹⁰, E. Salama^{11,12}

National Institute of Chemical Physics and Biophysics, Tallinn, Estonia

S. Bhowmik, A. Carvalho Antunes De Oliveira, R.K. Dewanjee, K. Ehataht, M. Kadastik, M. Raidal, C. Veelken

Department of Physics, University of Helsinki, Helsinki, Finland

P. Eerola, H. Kirschenmann, J. Pekkanen, M. Voutilainen

Helsinki Institute of Physics, Helsinki, Finland

J. Havukainen, J.K. Heikkilä, T. Järvinen, V. Karimäki, R. Kinnunen, T. Lampén, K. Lassila-Perini, S. Laurila, S. Lehti, T. Lindén, P. Luukka, T. Mäenpää, H. Siikonen, E. Tuominen, J. Tuominiemi

Lappeenranta University of Technology, Lappeenranta, Finland

T. Tuuva

IRFU, CEA, Université Paris-Saclay, Gif-sur-Yvette, France

M. Besancon, F. Couderc, M. Dejardin, D. Denegri, J.L. Faure, F. Ferri, S. Ganjour, A. Givernaud, P. Gras, G. Hamel de Monchenault, P. Jarry, C. Leloup, E. Locci, J. Malcles, G. Negro, J. Rander, A. Rosowsky, M.Ö. Sahin, M. Titov

Laboratoire Leprince-Ringuet, Ecole polytechnique, CNRS/IN2P3, Université Paris-Saclay, Palaiseau, France

A. Abdulsalam¹³, C. Amendola, I. Antropov, F. Beaudette, P. Busson, C. Charlot, R. Granier de Cassagnac, I. Kucher, A. Lobanov, J. Martin Blanco, C. Martin Perez, M. Nguyen, C. Ochando, G. Ortona, P. Pigard, J. Rembser, R. Salerno, J.B. Sauvan, Y. Sirois, A.G. Stahl Leiton, A. Zabi, A. Zghiche

Université de Strasbourg, CNRS, IPHC UMR 7178, Strasbourg, France

J.-L. Agram¹⁴, J. Andrea, D. Bloch, J.-M. Brom, E.C. Chabert, V. Cherepanov, C. Collard, E. Conte¹⁴, J.-C. Fontaine¹⁴, D. Gelé, U. Goerlach, M. Jansová, A.-C. Le Bihan, N. Tonon, P. Van Hove

Centre de Calcul de l'Institut National de Physique Nucleaire et de Physique des Particules, CNRS/IN2P3, Villeurbanne, France

S. Gadrat

Université de Lyon, Université Claude Bernard Lyon 1, CNRS-IN2P3, Institut de Physique Nucléaire de Lyon, Villeurbanne, France

S. Beauceron, C. Bernet, G. Boudoul, N. Chanon, R. Chierici, D. Contardo, P. Depasse, H. El Mamouni, J. Fay, L. Finco, S. Gascon, M. Gouzevitch, G. Grenier, B. Ille, F. Lagarde, I.B. Laktineh, H. Lattaud, M. Lethuillier, L. Mirabito, S. Perries, A. Popov¹⁵, V. Sordini, G. Touquet, M. Vander Donckt, S. Viret

Georgian Technical University, Tbilisi, Georgia

A. Khvedelidze⁸

Tbilisi State University, Tbilisi, Georgia

Z. Tsamalaidze⁸

RWTH Aachen University, I. Physikalisches Institut, Aachen, Germany

C. Autermann, L. Feld, M.K. Kiesel, K. Klein, M. Lipinski, M. Preuten, M.P. Rauch, C. Schomakers, J. Schulz, M. Teroerde, B. Wittmer

RWTH Aachen University, III. Physikalisches Institut A, Aachen, Germany

A. Albert, D. Duchardt, M. Erdmann, S. Erdweg, T. Esch, R. Fischer, S. Ghosh, A. Güth, T. Hebbeker, C. Heidemann, K. Hoepfner, H. Keller, L. Mastrolorenzo, M. Merschmeyer, A. Meyer, P. Millet, S. Mukherjee, T. Pook, M. Radziej, H. Reithler, M. Rieger, A. Schmidt, D. Teyssier, S. Thüer

RWTH Aachen University, III. Physikalisches Institut B, Aachen, Germany

G. Flügge, O. Hlushchenko, T. Kress, A. Künsken, T. Müller, A. Nehr Korn, A. Nowack, C. Pistone, O. Pooth, D. Roy, H. Sert, A. Stahl¹⁶

Deutsches Elektronen-Synchrotron, Hamburg, Germany

M. Aldaya Martin, T. Arndt, C. Asawatangtrakuldee, I. Babounikau, K. Beernaert, O. Behnke, U. Behrens, A. Bermúdez Martínez, D. Bertsche, A.A. Bin Anuar, K. Borras¹⁷, V. Botta, A. Campbell, P. Connor, C. Contreras-Campana, V. Danilov, A. De Wit, M.M. Defranchis, C. Diez Pardos, D. Domínguez Damiani, G. Eckerlin, T. Eichhorn, A. Elwood, E. Eren, E. Gallo¹⁸, A. Geiser, A. Grohsjean, M. Guthoff, M. Haranko, A. Harb, J. Hauk, H. Jung, M. Kasemann, J. Keaveney, C. Kleinwort, J. Knolle, D. Krücker, W. Lange, A. Lelek, T. Lenz, J. Leonard, K. Lipka, W. Lohmann¹⁹, R. Mankel, I.-A. Melzer-Pellmann, A.B. Meyer, M. Meyer, M. Missiroli, G. Mittag, J. Mnich, V. Myronenko, S.K. Pflitsch, D. Pitzl, A. Raspereza, M. Savitskyi, P. Saxena, P. Schütze, C. Schwanenberger, R. Shevchenko, A. Singh, H. Tholen, O. Turkot, A. Vagnerini, G.P. Van Onsem, R. Walsh, Y. Wen, K. Wichmann, C. Wissing, O. Zenaiev

University of Hamburg, Hamburg, Germany

R. Aggleton, S. Bein, L. Benato, A. Benecke, V. Blobel, T. Dreyer, A. Ebrahimi, E. Garutti, D. Gonzalez, P. Gunnellini, J. Haller, A. Hinzmann, A. Karavdina, G. Kasieczka, R. Klanner, R. Kogler, N. Kovalchuk, S. Kurz, V. Kutzner, J. Lange, D. Marconi, J. Multhaupt, M. Niedziela, C.E.N. Niemeyer, D. Nowatschin, A. Perieanu, A. Reimers, O. Rieger, C. Scharf, P. Schleper, S. Schumann, J. Schwandt, J. Sonneveld, H. Stadie, G. Steinbrück, F.M. Stober, M. Stöver, A. Vanhoefer, B. Vormwald, I. Zoi

Karlsruher Institut fuer Technologie, Karlsruhe, Germany

M. Akbiyik, C. Barth, M. Baselga, S. Baur, E. Butz, R. Caspart, T. Chwalek, F. Colombo, W. De Boer, A. Dierlamm, K. El Morabit, N. Faltermann, B. Freund, M. Giffels, M.A. Harrendorf, F. Hartmann¹⁶, S.M. Heindl, U. Husemann, F. Kassel¹⁶, I. Katkov¹⁵, S. Kudella, S. Mitra, M.U. Mozer, Th. Müller, M. Plagge, G. Quast, K. Rabbertz, M. Schröder, I. Shvetsov, G. Sieber, H.J. Simonis, R. Ulrich, S. Wayand, M. Weber, T. Weiler, S. Williamson, C. Wöhrmann, R. Wolf

Institute of Nuclear and Particle Physics (INPP), NCSR Demokritos, Aghia Paraskevi, Greece

G. Anagnostou, G. Daskalakis, T. Gerasis, A. Kyriakis, D. Loukas, G. Paspalaki, I. Topsis-Giotis

National and Kapodistrian University of Athens, Athens, Greece

G. Karathanasis, S. Kesisoglou, P. Kontaxakis, A. Panagiotou, I. Papavergou, N. Saoulidou, E. Tziaferi, K. Vellidis

National Technical University of Athens, Athens, Greece

K. Kousouris, I. Papakrivopoulos, G. Tsipolitis

University of Ioánnina, Ioánnina, Greece

I. Evangelou, C. Foudas, P. Giannelis, P. Katsoulis, P. Kokkas, S. Mallios, N. Manthos, I. Papadopoulos, E. Paradas, J. Strologas, F.A. Triantis, D. Tsitsonis

MTA-ELTE Lendület CMS Particle and Nuclear Physics Group, Eötvös Loránd University, Budapest, Hungary

M. Bartók²⁰, M. Csanad, N. Filipovic, P. Major, M.I. Nagy, G. Pasztor, O. Surányi, G.I. Veres

Wigner Research Centre for Physics, Budapest, Hungary

G. Bencze, C. Hajdu, D. Horvath²¹, Á. Hunyadi, F. Sikler, T.Á. Vámi, V. Veszpremi, G. Vesztergombi[†]

Institute of Nuclear Research ATOMKI, Debrecen, Hungary

N. Beni, S. Czellar, J. Karancsi²², A. Makovec, J. Molnar, Z. Szillasi

Institute of Physics, University of Debrecen, Debrecen, Hungary

P. Raics, Z.L. Trocsanyi, B. Ujvari

Indian Institute of Science (IISc), Bangalore, India

S. Choudhury, J.R. Komaragiri, P.C. Tiwari

National Institute of Science Education and Research, HBNI, Bhubaneswar, India

S. Bahinipati²³, C. Kar, P. Mal, K. Mandal, A. Nayak²⁴, D.K. Sahoo²³, S.K. Swain

Panjab University, Chandigarh, India

S. Bansal, S.B. Beri, V. Bhatnagar, S. Chauhan, R. Chawla, N. Dhingra, R. Gupta, A. Kaur, M. Kaur, S. Kaur, R. Kumar, P. Kumari, M. Lohan, A. Mehta, K. Sandeep, S. Sharma, J.B. Singh, A.K. Viridi, G. Walia

University of Delhi, Delhi, India

A. Bhardwaj, B.C. Choudhary, R.B. Garg, M. Gola, S. Keshri, Ashok Kumar, S. Malhotra, M. Naimuddin, P. Priyanka, K. Ranjan, Aashaq Shah, R. Sharma

Saha Institute of Nuclear Physics, HBNI, Kolkata, India

R. Bhardwaj²⁵, M. Bharti²⁵, R. Bhattacharya, S. Bhattacharya, U. Bhawandeep²⁵, D. Bhowmik, S. Dey, S. Dutt²⁵, S. Dutta, S. Ghosh, K. Mondal, S. Nandan, A. Purohit, P.K. Rout, A. Roy, S. Roy Chowdhury, G. Saha, S. Sarkar, M. Sharan, B. Singh²⁵, S. Thakur²⁵

Indian Institute of Technology Madras, Madras, India

P.K. Behera

Bhabha Atomic Research Centre, Mumbai, India

R. Chudasama, D. Dutta, V. Jha, V. Kumar, P.K. Netrakanti, L.M. Pant, P. Shukla

Tata Institute of Fundamental Research-A, Mumbai, India

T. Aziz, M.A. Bhat, S. Dugad, G.B. Mohanty, N. Sur, B. Sutar, RavindraKumar Verma

Tata Institute of Fundamental Research-B, Mumbai, India

S. Banerjee, S. Bhattacharya, S. Chatterjee, P. Das, M. Guchait, Sa. Jain, S. Karmakar, S. Kumar, M. Maity²⁶, G. Majumder, K. Mazumdar, N. Sahoo, T. Sarkar²⁶

Indian Institute of Science Education and Research (IISER), Pune, India

S. Chauhan, S. Dube, V. Hegde, A. Kapoor, K. Kothekar, S. Pandey, A. Rane, S. Sharma

Institute for Research in Fundamental Sciences (IPM), Tehran, Iran

S. Chenarani²⁷, E. Eskandari Tadavani, S.M. Etesami²⁷, M. Khakzad, M. Mohammadi Najafabadi, M. Naseri, F. Rezaei Hosseinabadi, B. Safarzadeh²⁸, M. Zeinali

University College Dublin, Dublin, Ireland

M. Felcini, M. Grunewald

INFN Sezione di Bari ^a, Università di Bari ^b, Politecnico di Bari ^c, Bari, Italy

M. Abbrescia^{a,b}, C. Calabria^{a,b}, A. Colaleo^a, D. Creanza^{a,c}, L. Cristella^{a,b}, N. De Filippis^{a,c}, M. De Palma^{a,b}, A. Di Florio^{a,b}, F. Errico^{a,b}, L. Fiore^a, A. Gelmi^{a,b}, G. Iaselli^{a,c}, M. Ince^{a,b}, S. Lezki^{a,b}, G. Maggi^{a,c}, M. Maggi^a, G. Miniello^{a,b}, S. My^{a,b}, S. Nuzzo^{a,b}, A. Pompili^{a,b},

G. Pugliese^{a,c}, R. Radogna^a, A. Ranieri^a, G. Selvaggi^{a,b}, A. Sharma^a, L. Silvestris^a, R. Venditti^a, P. Verwilligen^a, G. Zito^a

INFN Sezione di Bologna ^a, Università di Bologna ^b, Bologna, Italy

G. Abbiendi^a, C. Battilana^{a,b}, D. Bonacorsi^{a,b}, L. Borgonovi^{a,b}, S. Braibant-Giacomelli^{a,b}, R. Campanini^{a,b}, P. Capiluppi^{a,b}, A. Castro^{a,b}, F.R. Cavallo^a, S.S. Chhibra^{a,b}, C. Ciocca^a, G. Codispoti^{a,b}, M. Cuffiani^{a,b}, G.M. Dallavalle^a, F. Fabbri^a, A. Fanfani^{a,b}, E. Fontanesi, P. Giacomelli^a, C. Grandi^a, L. Guiducci^{a,b}, S. Lo Meo^a, S. Marcellini^a, G. Masetti^a, A. Montanari^a, F.L. Navarria^{a,b}, A. Perrotta^a, F. Primavera^{a,b,16}, A.M. Rossi^{a,b}, T. Rovelli^{a,b}, G.P. Siroli^{a,b}, N. Tosi^a

INFN Sezione di Catania ^a, Università di Catania ^b, Catania, Italy

S. Albergo^{a,b}, A. Di Mattia^a, R. Potenza^{a,b}, A. Tricomi^{a,b}, C. Tuve^{a,b}

INFN Sezione di Firenze ^a, Università di Firenze ^b, Firenze, Italy

G. Barbagli^a, K. Chatterjee^{a,b}, V. Ciulli^{a,b}, C. Civinini^a, R. D'Alessandro^{a,b}, E. Focardi^{a,b}, G. Latino, P. Lenzi^{a,b}, M. Meschini^a, S. Paoletti^a, L. Russo^{a,29}, G. Sguazzoni^a, D. Strom^a, L. Viliani^a

INFN Laboratori Nazionali di Frascati, Frascati, Italy

L. Benussi, S. Bianco, F. Fabbri, D. Piccolo

INFN Sezione di Genova ^a, Università di Genova ^b, Genova, Italy

F. Ferro^a, F. Ravera^{a,b}, E. Robutti^a, S. Tosi^{a,b}

INFN Sezione di Milano-Bicocca ^a, Università di Milano-Bicocca ^b, Milano, Italy

A. Benaglia^a, A. Beschi^b, F. Brivio^{a,b}, V. Ciriolo^{a,b,16}, S. Di Guida^{a,d,16}, M.E. Dinardo^{a,b}, S. Fiorendi^{a,b}, S. Gennai^a, A. Ghezzi^{a,b}, P. Govoni^{a,b}, M. Malberti^{a,b}, S. Malvezzi^a, A. Massironi^{a,b}, D. Menasce^a, F. Monti, L. Moroni^a, M. Paganoni^{a,b}, D. Pedrini^a, S. Ragazzi^{a,b}, T. Tabarelli de Fatis^{a,b}, D. Zuolo^{a,b}

INFN Sezione di Napoli ^a, Università di Napoli 'Federico II' ^b, Napoli, Italy, Università della Basilicata ^c, Potenza, Italy, Università G. Marconi ^d, Roma, Italy

S. Buontempo^a, N. Cavallo^{a,c}, A. De Iorio^{a,b}, A. Di Crescenzo^{a,b}, F. Fabozzi^{a,c}, F. Fienga^a, G. Galati^a, A.O.M. Iorio^{a,b}, W.A. Khan^a, L. Lista^a, S. Meola^{a,d,16}, P. Paolucci^{a,16}, C. Sciacca^{a,b}, E. Voevodina^{a,b}

INFN Sezione di Padova ^a, Università di Padova ^b, Padova, Italy, Università di Trento ^c, Trento, Italy

P. Azzi^a, N. Bacchetta^a, A. Boletti^{a,b}, A. Bragagnolo, R. Carlin^{a,b}, P. Checchia^a, M. Dall'Osso^{a,b}, P. De Castro Manzano^a, T. Dorigo^a, U. Dosselli^a, F. Gasparini^{a,b}, U. Gasparini^{a,b}, A. Gozzelino^a, S.Y. Hoh, S. Lacaprara^a, P. Lujan, M. Margoni^{a,b}, A.T. Meneguzzo^{a,b}, J. Pazzini^{a,b}, N. Pozzobon^{a,b}, P. Ronchese^{a,b}, R. Rossin^{a,b}, F. Simonetto^{a,b}, A. Tiko, E. Torassa^a, S. Ventura^a, M. Zanetti^{a,b}, P. Zotto^{a,b}

INFN Sezione di Pavia ^a, Università di Pavia ^b, Pavia, Italy

A. Braghieri^a, A. Magnani^a, P. Montagna^{a,b}, S.P. Ratti^{a,b}, V. Re^a, M. Ressegotti^{a,b}, C. Riccardi^{a,b}, P. Salvini^a, I. Vai^{a,b}, P. Vitulo^{a,b}

INFN Sezione di Perugia ^a, Università di Perugia ^b, Perugia, Italy

M. Biasini^{a,b}, G.M. Bilei^a, C. Cecchi^{a,b}, D. Ciangottini^{a,b}, L. Fanò^{a,b}, P. Lariccia^{a,b}, R. Leonardi^{a,b}, E. Manoni^a, G. Mantovani^{a,b}, V. Mariani^{a,b}, M. Menichelli^a, A. Rossi^{a,b}, A. Santocchia^{a,b}, D. Spiga^a

INFN Sezione di Pisa ^a, Università di Pisa ^b, Scuola Normale Superiore di Pisa ^c, Pisa, Italy

K. Androsov^a, P. Azzurri^a, G. Bagliesi^a, L. Bianchini^a, T. Boccali^a, L. Borrello, R. Castaldi^a, M.A. Ciocci^{a,b}, R. Dell'Orso^a, G. Fedi^a, F. Fiori^{a,c}, L. Giannini^{a,c}, A. Giassi^a, M.T. Grippo^a, F. Ligabue^{a,c}, E. Manca^{a,c}, G. Mandorli^{a,c}, A. Messineo^{a,b}, F. Palla^a, A. Rizzi^{a,b}, P. Spagnolo^a, R. Tenchini^a, G. Tonelli^{a,b}, A. Venturi^a, P.G. Verdini^a

INFN Sezione di Roma ^a, Sapienza Università di Roma ^b, Rome, Italy

L. Barone^{a,b}, F. Cavallari^a, M. Cipriani^{a,b}, D. Del Re^{a,b}, E. Di Marco^{a,b}, M. Diemoz^a, S. Gelli^{a,b}, E. Longo^{a,b}, B. Marzocchi^{a,b}, P. Meridiani^a, G. Organtini^{a,b}, F. Pandolfi^a, R. Paramatti^{a,b}, F. Preiato^{a,b}, S. Rahatlou^{a,b}, C. Rovelli^a, F. Santanastasio^{a,b}

INFN Sezione di Torino ^a, Università di Torino ^b, Torino, Italy, Università del Piemonte Orientale ^c, Novara, Italy

N. Amapane^{a,b}, R. Arcidiacono^{a,c}, S. Argiro^{a,b}, M. Arneodo^{a,c}, N. Bartosik^a, R. Bellan^{a,b}, C. Biino^a, N. Cartiglia^a, F. Cenna^{a,b}, S. Cometti^a, M. Costa^{a,b}, R. Covarelli^{a,b}, N. Demaria^a, B. Kiani^{a,b}, C. Mariotti^a, S. Maselli^a, E. Migliore^{a,b}, V. Monaco^{a,b}, E. Monteil^{a,b}, M. Monteno^a, M.M. Obertino^{a,b}, L. Pacher^{a,b}, N. Pastrone^a, M. Pelliccioni^a, G.L. Pinna Angioni^{a,b}, A. Romero^{a,b}, M. Ruspa^{a,c}, R. Sacchi^{a,b}, K. Shchelina^{a,b}, V. Sola^a, A. Solano^{a,b}, D. Soldi^{a,b}, A. Staiano^a

INFN Sezione di Trieste ^a, Università di Trieste ^b, Trieste, Italy

S. Belforte^a, V. Candelise^{a,b}, M. Casarsa^a, F. Cossutti^a, A. Da Rold^{a,b}, G. Della Ricca^{a,b}, F. Vazzoler^{a,b}, A. Zanetti^a

Kyungpook National University, Daegu, Korea

D.H. Kim, G.N. Kim, M.S. Kim, J. Lee, S. Lee, S.W. Lee, C.S. Moon, Y.D. Oh, S.I. Pak, S. Sekmen, D.C. Son, Y.C. Yang

Chonnam National University, Institute for Universe and Elementary Particles, Kwangju, Korea

H. Kim, D.H. Moon, G. Oh

Hanyang University, Seoul, Korea

B. Francois, J. Goh³⁰, T.J. Kim

Korea University, Seoul, Korea

S. Cho, S. Choi, Y. Go, D. Gyun, S. Ha, B. Hong, Y. Jo, K. Lee, K.S. Lee, S. Lee, J. Lim, S.K. Park, Y. Roh

Sejong University, Seoul, Korea

H.S. Kim

Seoul National University, Seoul, Korea

J. Almond, J. Kim, J.S. Kim, H. Lee, K. Lee, K. Nam, S.B. Oh, B.C. Radburn-Smith, S.h. Seo, U.K. Yang, H.D. Yoo, G.B. Yu

University of Seoul, Seoul, Korea

D. Jeon, H. Kim, J.H. Kim, J.S.H. Lee, I.C. Park

Sungkyunkwan University, Suwon, Korea

Y. Choi, C. Hwang, J. Lee, I. Yu

Vilnius University, Vilnius, Lithuania

V. Dudenas, A. Juodagalvis, J. Vaitkus

National Centre for Particle Physics, Universiti Malaya, Kuala Lumpur, Malaysia

I. Ahmed, Z.A. Ibrahim, M.A.B. Md Ali³¹, F. Mohamad Idris³², W.A.T. Wan Abdullah, M.N. Yusli, Z. Zolkapli

Universidad de Sonora (UNISON), Hermosillo, Mexico

J.F. Benitez, A. Castaneda Hernandez, J.A. Murillo Quijada

Centro de Investigacion y de Estudios Avanzados del IPN, Mexico City, Mexico

H. Castilla-Valdez, E. De La Cruz-Burelo, M.C. Duran-Osuna, I. Heredia-De La Cruz³³, R. Lopez-Fernandez, J. Mejia Guisao, R.I. Rabadan-Trejo, M. Ramirez-Garcia, G. Ramirez-Sanchez, R Reyes-Almanza, A. Sanchez-Hernandez

Universidad Iberoamericana, Mexico City, Mexico

S. Carrillo Moreno, C. Oropeza Barrera, F. Vazquez Valencia

Benemerita Universidad Autonoma de Puebla, Puebla, Mexico

J. Eysermans, I. Pedraza, H.A. Salazar Ibarguen, C. Uribe Estrada

Universidad Autónoma de San Luis Potosí, San Luis Potosí, Mexico

A. Morelos Pineda

University of Auckland, Auckland, New Zealand

D. Krofcheck

University of Canterbury, Christchurch, New Zealand

S. Bheesette, P.H. Butler

National Centre for Physics, Quaid-I-Azam University, Islamabad, Pakistan

A. Ahmad, M. Ahmad, M.I. Asghar, Q. Hassan, H.R. Hoorani, A. Saddique, M.A. Shah, M. Shoaib, M. Waqas

National Centre for Nuclear Research, Swierk, Poland

H. Bialkowska, M. Bluj, B. Boimska, T. Frueboes, M. Górski, M. Kazana, M. Szeleper, P. Traczyk, P. Zalewski

Institute of Experimental Physics, Faculty of Physics, University of Warsaw, Warsaw, Poland

K. Bunkowski, A. Byszuk³⁴, K. Doroba, A. Kalinowski, M. Konecki, J. Krolikowski, M. Misiura, M. Olszewski, A. Pyskir, M. Walczak

Laboratório de Instrumentação e Física Experimental de Partículas, Lisboa, Portugal

M. Araujo, P. Bargassa, C. Beirão Da Cruz E Silva, A. Di Francesco, P. Faccioli, B. Galinhas, M. Gallinaro, J. Hollar, N. Leonardo, M.V. Nemallapudi, J. Seixas, G. Strong, O. Toldaiev, D. Vadrucio, J. Varela

Joint Institute for Nuclear Research, Dubna, Russia

S. Afanasiev, P. Bunin, M. Gavrilenko, I. Golutvin, I. Gorbunov, A. Kamenev, V. Karjavine, A. Lanev, A. Malakhov, V. Matveev^{35,36}, P. Moiseenz, V. Palichik, V. Perelygin, S. Shmatov, S. Shulha, N. Skatchkov, V. Smirnov, N. Voytishin, A. Zarubin

Petersburg Nuclear Physics Institute, Gatchina (St. Petersburg), Russia

V. Golovtsov, Y. Ivanov, V. Kim³⁷, E. Kuznetsova³⁸, P. Levchenko, V. Murzin, V. Oreshkin, I. Smirnov, D. Sosnov, V. Sulimov, L. Uvarov, S. Vavilov, A. Vorobyev

Institute for Nuclear Research, Moscow, Russia

Yu. Andreev, A. Dermenev, S. Gninenko, N. Golubev, A. Karneyeu, M. Kirsanov, N. Krasnikov, A. Pashenkov, D. Tlisov, A. Toropin

Institute for Theoretical and Experimental Physics, Moscow, Russia

V. Epshteyn, V. Gavrilov, N. Lychkovskaya, V. Popov, I. Pozdnyakov, G. Safronov, A. Spiridonov, A. Stepenov, V. Stolin, M. Toms, E. Vlasov, A. Zhokin

Moscow Institute of Physics and Technology, Moscow, Russia

T. Aushev

National Research Nuclear University 'Moscow Engineering Physics Institute' (MEPhI), Moscow, Russia

R. Chistov³⁹, M. Danilov³⁹, P. Parygin, D. Philippov, S. Polikarpov³⁹, E. Tarkovskii

P.N. Lebedev Physical Institute, Moscow, Russia

V. Andreev, M. Azarkin, I. Dremin³⁶, M. Kirakosyan, S.V. Rusakov, A. Terkulov

Skobeltsyn Institute of Nuclear Physics, Lomonosov Moscow State University, Moscow, Russia

A. Baskakov, A. Belyaev, E. Boos, M. Dubinin⁴⁰, L. Dudko, A. Ershov, A. Gribushin, V. Klyukhin, O. Kodolova, I. Lokhtin, I. Miagkov, S. Obraztsov, S. Petrushanko, V. Savrin, A. Snigirev

Novosibirsk State University (NSU), Novosibirsk, Russia

A. Barnyakov⁴¹, V. Blinov⁴¹, T. Dimova⁴¹, L. Kardapol'tsev⁴¹, Y. Skovpen⁴¹

Institute for High Energy Physics of National Research Centre 'Kurchatov Institute', Protvino, Russia

I. Azhgirey, I. Bayshev, S. Bitioukov, D. Elumakhov, A. Godizov, V. Kachanov, A. Kalinin, D. Konstantinov, P. Mandrik, V. Petrov, R. Ryutin, S. Slabospitskii, A. Sobol, S. Troshin, N. Tyurin, A. Uzunian, A. Volkov

National Research Tomsk Polytechnic University, Tomsk, Russia

A. Babaev, S. Baidali, V. Okhotnikov

University of Belgrade, Faculty of Physics and Vinca Institute of Nuclear Sciences, Belgrade, Serbia

P. Adzic⁴², P. Cirkovic, D. Devetak, M. Dordevic, J. Milosevic

Centro de Investigaciones Energéticas Medioambientales y Tecnológicas (CIEMAT), Madrid, Spain

J. Alcaraz Maestre, A. Álvarez Fernández, I. Bachiller, M. Barrio Luna, J.A. Brochero Cifuentes, M. Cerrada, N. Colino, B. De La Cruz, A. Delgado Peris, C. Fernandez Bedoya, J.P. Fernández Ramos, J. Flix, M.C. Fouz, O. Gonzalez Lopez, S. Goy Lopez, J.M. Hernandez, M.I. Josa, D. Moran, A. Pérez-Calero Yzquierdo, J. Puerta Pelayo, I. Redondo, L. Romero, M.S. Soares, A. Triossi

Universidad Autónoma de Madrid, Madrid, Spain

C. Albajar, J.F. de Trocóniz

Universidad de Oviedo, Oviedo, Spain

J. Cuevas, C. Erice, J. Fernandez Menendez, S. Folgueras, I. Gonzalez Caballero, J.R. González Fernández, E. Palencia Cortezon, V. Rodríguez Bouza, S. Sanchez Cruz, P. Vischia, J.M. Vizan Garcia

Instituto de Física de Cantabria (IFCA), CSIC-Universidad de Cantabria, Santander, Spain

I.J. Cabrillo, A. Calderon, B. Chazin Quero, J. Duarte Campderros, M. Fernandez, P.J. Fernández Manteca, A. García Alonso, J. Garcia-Ferrero, G. Gomez, A. Lopez Virto,

J. Marco, C. Martinez Rivero, P. Martinez Ruiz del Arbol, F. Matorras, J. Piedra Gomez, C. Prieels, T. Rodrigo, A. Ruiz-Jimeno, L. Scodellaro, N. Trevisani, I. Vila, R. Vilar Cortabitarte

University of Ruhuna, Department of Physics, Matara, Sri Lanka

N. Wickramage

CERN, European Organization for Nuclear Research, Geneva, Switzerland

D. Abbaneo, B. Akgun, E. Auffray, G. Auzinger, P. Baillon, A.H. Ball, D. Barney, J. Bendavid, M. Bianco, A. Bocci, C. Botta, E. Brondolin, T. Camporesi, M. Cepeda, G. Cerminara, E. Chapon, Y. Chen, G. Cucciati, D. d'Enterria, A. Dabrowski, N. Daci, V. Daponte, A. David, A. De Roeck, N. Deelen, M. Dobson, M. Dünser, N. Dupont, A. Elliott-Peisert, P. Everaerts, F. Fallavollita⁴³, D. Fasanella, G. Franzoni, J. Fulcher, W. Funk, D. Gigi, A. Gilbert, K. Gill, F. Glege, M. Guilbaud, D. Gulhan, J. Hegeman, C. Heidegger, V. Innocente, A. Jafari, P. Janot, O. Karacheban¹⁹, J. Kieseler, A. Kornmayer, M. Krammer¹, C. Lange, P. Lecoq, C. Lourenço, L. Malgeri, M. Mannelli, F. Meijers, J.A. Merlin, S. Mersi, E. Meschi, P. Milenovic⁴⁴, F. Moortgat, M. Mulders, J. Ngadiuba, S. Nourbakhsh, S. Orfanelli, L. Orsini, F. Pantaleo¹⁶, L. Pape, E. Perez, M. Peruzzi, A. Petrilli, G. Petrucciani, A. Pfeiffer, M. Pierini, F.M. Pitters, D. Rabady, A. Racz, T. Reis, G. Rolandi⁴⁵, M. Rovere, H. Sakulin, C. Schäfer, C. Schwick, M. Seidel, M. Selvaggi, A. Sharma, P. Silva, P. Sphicas⁴⁶, A. Stakia, J. Steggemann, M. Tosi, D. Treille, A. Tsirou, V. Veckalns⁴⁷, M. Verzetti, W.D. Zeuner

Paul Scherrer Institut, Villigen, Switzerland

L. Caminada⁴⁸, K. Deiters, W. Erdmann, R. Horisberger, Q. Ingram, H.C. Kaestli, D. Kotlinski, U. Langenegger, T. Rohe, S.A. Wiederkehr

ETH Zurich - Institute for Particle Physics and Astrophysics (IPA), Zurich, Switzerland

M. Backhaus, L. Bäni, P. Berger, N. Chernyavskaya, G. Dissertori, M. Dittmar, M. Donegà, C. Dorfer, T.A. Gómez Espinosa, C. Grab, D. Hits, T. Klijnsma, W. Luster, R.A. Manzoni, M. Marionneau, M.T. Meinhard, F. Micheli, P. Musella, F. Nessi-Tedaldi, J. Pata, F. Pauss, G. Perrin, L. Perrozzi, S. Pigazzini, M. Quittnat, C. Reissel, D. Ruini, D.A. Sanz Becerra, M. Schönenberger, L. Shchutska, V.R. Tavolaro, K. Theofilatos, M.L. Vesterbacka Olsson, R. Wallny, D.H. Zhu

Universität Zürich, Zurich, Switzerland

T.K. Aarrestad, C. Amsler⁴⁹, D. Brzhechko, M.F. Canelli, A. De Cosa, R. Del Burgo, S. Donato, C. Galloni, T. Hreus, B. Kilminster, S. Leontsinis, I. Neutelings, G. Rauco, P. Robmann, D. Salerno, K. Schweiger, C. Seitz, Y. Takahashi, A. Zucchetta

National Central University, Chung-Li, Taiwan

Y.H. Chang, K.y. Cheng, T.H. Doan, R. Khurana, C.M. Kuo, W. Lin, A. Pozdnyakov, S.S. Yu

National Taiwan University (NTU), Taipei, Taiwan

P. Chang, Y. Chao, K.F. Chen, P.H. Chen, W.-S. Hou, Arun Kumar, Y.F. Liu, R.-S. Lu, E. Paganis, A. Psallidas, A. Steen

Chulalongkorn University, Faculty of Science, Department of Physics, Bangkok, Thailand

B. Asavapibhop, N. Srimanobhas, N. Suwonjandee

Çukurova University, Physics Department, Science and Art Faculty, Adana, Turkey

A. Bat, F. Boran, S. Damarseckin, Z.S. Demiroglu, F. Dolek, C. Dozen, I. Dumanoglu, E. Eskut, S. Girgis, G. Gokbulut, Y. Guler, E. Gurpinar, I. Hos⁵⁰, C. Isik, E.E. Kangal⁵¹, O. Kara, A. Kayis Topaksu, U. Kiminsu, M. Oglakci, G. Onengut, K. Ozdemir⁵², D. Sunar Cerci⁵³, B. Tali⁵³, U.G. Tok, H. Topakli⁵⁴, S. Turkcapar, I.S. Zorbakir, C. Zorbilmez

Middle East Technical University, Physics Department, Ankara, Turkey

B. Isildak⁵⁵, G. Karapinar⁵⁶, M. Yalvac, M. Zeyrek

Bogazici University, Istanbul, Turkey

I.O. Atakisi, E. Gülmez, M. Kaya⁵⁷, O. Kaya⁵⁸, S. Ozkorucuklu⁵⁹, S. Tekten, E.A. Yetkin⁶⁰

Istanbul Technical University, Istanbul, Turkey

M.N. Agaras, A. Cakir, K. Cankocak, Y. Komurcu, S. Sen⁶¹

Institute for Scintillation Materials of National Academy of Science of Ukraine, Kharkov, Ukraine

B. Grynyov

National Scientific Center, Kharkov Institute of Physics and Technology, Kharkov, Ukraine

L. Levchuk

University of Bristol, Bristol, United Kingdom

F. Ball, L. Beck, J.J. Brooke, D. Burns, E. Clement, D. Cussans, O. Davignon, H. Flacher, J. Goldstein, G.P. Heath, H.F. Heath, L. Kreczko, D.M. Newbold⁶², S. Paramesvaran, B. Penning, T. Sakuma, D. Smith, V.J. Smith, J. Taylor, A. Titterton

Rutherford Appleton Laboratory, Didcot, United Kingdom

K.W. Bell, A. Belyaev⁶³, C. Brew, R.M. Brown, D. Cieri, D.J.A. Cockerill, J.A. Coughlan, K. Harder, S. Harper, J. Linacre, E. Olaiya, D. Petyt, C.H. Shepherd-Themistocleous, A. Thea, I.R. Tomalin, T. Williams, W.J. Womersley

Imperial College, London, United Kingdom

R. Bainbridge, P. Bloch, J. Borg, S. Breeze, O. Buchmuller, A. Bundock, D. Colling, P. Dauncey, G. Davies, M. Della Negra, R. Di Maria, Y. Haddad, G. Hall, G. Iles, T. James, M. Komm, C. Laner, L. Lyons, A.-M. Magnan, S. Malik, A. Martelli, J. Nash⁶⁴, A. Nikitenko⁷, V. Palladino, M. Pesaresi, D.M. Raymond, A. Richards, A. Rose, E. Scott, C. Seez, A. Shtipliyski, G. Singh, M. Stoye, T. Strebler, S. Summers, A. Tapper, K. Uchida, T. Virdee¹⁶, N. Wardle, D. Winterbottom, J. Wright, S.C. Zenz

Brunel University, Uxbridge, United Kingdom

J.E. Cole, P.R. Hobson, A. Khan, P. Kyberd, C.K. Mackay, A. Morton, I.D. Reid, L. Teodorescu, S. Zahid

Baylor University, Waco, USA

K. Call, J. Dittmann, K. Hatakeyama, H. Liu, C. Madrid, B. McMaster, N. Pastika, C. Smith

Catholic University of America, Washington DC, USA

R. Bartek, A. Dominguez

The University of Alabama, Tuscaloosa, USA

A. Buccilli, S.I. Cooper, C. Henderson, P. Rumerio, C. West

Boston University, Boston, USA

D. Arcaro, T. Bose, D. Gastler, D. Pinna, D. Rankin, C. Richardson, J. Rohlf, L. Sulak, D. Zou

Brown University, Providence, USA

G. Benelli, X. Coubez, D. Cutts, M. Hadley, J. Hakala, U. Heintz, J.M. Hogan⁶⁵, K.H.M. Kwok, E. Laird, G. Landsberg, J. Lee, Z. Mao, M. Narain, S. Sagir⁶⁶, R. Syarif, E. Usai, D. Yu

University of California, Davis, Davis, USA

R. Band, C. Brainerd, R. Breedon, D. Burns, M. Calderon De La Barca Sanchez, M. Chertok,

J. Conway, R. Conway, P.T. Cox, R. Erbacher, C. Flores, G. Funk, W. Ko, O. Kukral, R. Lander, M. Mulhearn, D. Pellett, J. Pilot, S. Shalhout, M. Shi, D. Stolp, D. Taylor, K. Tos, M. Tripathi, Z. Wang, F. Zhang

University of California, Los Angeles, USA

M. Bachtis, C. Bravo, R. Cousins, A. Dasgupta, A. Florent, J. Hauser, M. Ignatenko, N. Mccoll, S. Regnard, D. Saltzberg, C. Schnaible, V. Valuev

University of California, Riverside, Riverside, USA

E. Bouvier, K. Burt, R. Clare, J.W. Gary, S.M.A. Ghiasi Shirazi, G. Hanson, G. Karapostoli, E. Kennedy, F. Lacroix, O.R. Long, M. Olmedo Negrete, M.I. Paneva, W. Si, L. Wang, H. Wei, S. Wimpenny, B.R. Yates

University of California, San Diego, La Jolla, USA

J.G. Branson, P. Chang, S. Cittolin, M. Derdzinski, R. Gerosa, D. Gilbert, B. Hashemi, A. Holzner, D. Klein, G. Kole, V. Krutelyov, J. Letts, M. Masciovecchio, D. Olivito, S. Padhi, M. Pieri, M. Sani, V. Sharma, S. Simon, M. Tadel, A. Vartak, S. Wasserbaech⁶⁷, J. Wood, F. Würthwein, A. Yagil, G. Zevi Della Porta

University of California, Santa Barbara - Department of Physics, Santa Barbara, USA

N. Amin, R. Bhandari, J. Bradmiller-Feld, C. Campagnari, M. Citron, A. Dishaw, V. Dutta, M. Franco Sevilla, L. Gouskos, R. Heller, J. Incandela, A. Ovcharova, H. Qu, J. Richman, D. Stuart, I. Suarez, S. Wang, J. Yoo

California Institute of Technology, Pasadena, USA

D. Anderson, A. Bornheim, J.M. Lawhorn, H.B. Newman, T.Q. Nguyen, M. Spiropulu, J.R. Vlimant, R. Wilkinson, S. Xie, Z. Zhang, R.Y. Zhu

Carnegie Mellon University, Pittsburgh, USA

M.B. Andrews, T. Ferguson, T. Mudholkar, M. Paulini, M. Sun, I. Vorobiev, M. Weinberg

University of Colorado Boulder, Boulder, USA

J.P. Cumalat, W.T. Ford, F. Jensen, A. Johnson, M. Krohn, E. MacDonald, T. Mulholland, R. Patel, A. Perloff, K. Stenson, K.A. Ulmer, S.R. Wagner

Cornell University, Ithaca, USA

J. Alexander, J. Chaves, Y. Cheng, J. Chu, A. Datta, K. Mcdermott, N. Mirman, J.R. Patterson, D. Quach, A. Rinkevicius, A. Ryd, L. Skinnari, L. Soffi, S.M. Tan, Z. Tao, J. Thom, J. Tucker, P. Wittich, M. Zientek

Fermi National Accelerator Laboratory, Batavia, USA

S. Abdullin, M. Albrow, M. Alyari, G. Apollinari, A. Apresyan, A. Apyan, S. Banerjee, L.A.T. Bauerdick, A. Beretvas, J. Berryhill, P.C. Bhat, K. Burkett, J.N. Butler, A. Canepa, G.B. Cerati, H.W.K. Cheung, F. Chlebana, M. Cremonesi, J. Duarte, V.D. Elvira, J. Freeman, Z. Gecse, E. Gottschalk, L. Gray, D. Green, S. Grünendahl, O. Gutsche, J. Hanlon, R.M. Harris, S. Hasegawa, J. Hirschauer, Z. Hu, B. Jayatilaka, S. Jindariani, M. Johnson, U. Joshi, B. Klima, M.J. Kortelainen, B. Kreis, S. Lammel, D. Lincoln, R. Lipton, M. Liu, T. Liu, J. Lykken, K. Maeshima, J.M. Marraffino, D. Mason, P. McBride, P. Merkel, S. Mrenna, S. Nahn, V. O'Dell, K. Pedro, C. Pena, O. Prokofyev, G. Rakness, L. Ristori, A. Savoy-Navarro⁶⁸, B. Schneider, E. Sexton-Kennedy, A. Soha, W.J. Spalding, L. Spiegel, S. Stoynev, J. Strait, N. Strobbe, L. Taylor, S. Tkaczyk, N.V. Tran, L. Uplegger, E.W. Vaandering, C. Vernieri, M. Verzocchi, R. Vidal, M. Wang, H.A. Weber, A. Whitbeck

University of Florida, Gainesville, USA

D. Acosta, P. Avery, P. Bortignon, D. Bourilkov, A. Brinkerhoff, L. Cadamuro, A. Carnes, M. Carver, D. Curry, R.D. Field, S.V. Gleyzer, B.M. Joshi, J. Konigsberg, A. Korytov, K.H. Lo, P. Ma, K. Matchev, H. Mei, G. Mitselmakher, D. Rosenzweig, K. Shi, D. Sperka, J. Wang, S. Wang, X. Zuo

Florida International University, Miami, USA

Y.R. Joshi, S. Linn

Florida State University, Tallahassee, USA

A. Ackert, T. Adams, A. Askew, S. Hagopian, V. Hagopian, K.F. Johnson, T. Kolberg, G. Martinez, T. Perry, H. Prosper, A. Saha, C. Schiber, R. Yohay

Florida Institute of Technology, Melbourne, USA

M.M. Baarmand, V. Bhopatkar, S. Colafranceschi, M. Hohlmann, D. Noonan, M. Rahmani, T. Roy, F. Yumiceva

University of Illinois at Chicago (UIC), Chicago, USA

M.R. Adams, L. Apanasevich, D. Berry, R.R. Betts, R. Cavanaugh, X. Chen, S. Dittmer, O. Evdokimov, C.E. Gerber, D.A. Hangal, D.J. Hofman, K. Jung, J. Kamin, C. Mills, I.D. Sandoval Gonzalez, M.B. Tonjes, H. Trauger, N. Varelas, H. Wang, X. Wang, Z. Wu, J. Zhang

The University of Iowa, Iowa City, USA

M. Alhousseini, B. Bilki⁶⁹, W. Clarida, K. Dilsiz⁷⁰, S. Durgut, R.P. Gandrajula, M. Haytmyradov, V. Khristenko, J.-P. Merlo, A. Mestvirishvili, A. Moeller, J. Nachtman, H. Ogul⁷¹, Y. Onel, F. Ozok⁷², A. Penzo, C. Snyder, E. Tiras, J. Wetzel

Johns Hopkins University, Baltimore, USA

B. Blumenfeld, A. Cocoros, N. Eminizer, D. Fehling, L. Feng, A.V. Gritsan, W.T. Hung, P. Maksimovic, J. Roskes, U. Sarica, M. Swartz, M. Xiao, C. You

The University of Kansas, Lawrence, USA

A. Al-bataineh, P. Baringer, A. Bean, S. Boren, J. Bowen, A. Bylinkin, J. Castle, S. Khalil, A. Kropivnitskaya, D. Majumder, W. Mcbrayer, M. Murray, C. Rogan, S. Sanders, E. Schmitz, J.D. Tapia Takaki, Q. Wang

Kansas State University, Manhattan, USA

S. Duric, A. Ivanov, K. Kaadze, D. Kim, Y. Maravin, D.R. Mendis, T. Mitchell, A. Modak, A. Mohammadi, L.K. Saini, N. Skhirtladze

Lawrence Livermore National Laboratory, Livermore, USA

F. Rebassoo, D. Wright

University of Maryland, College Park, USA

A. Baden, O. Baron, A. Belloni, S.C. Eno, Y. Feng, C. Ferraioli, N.J. Hadley, S. Jabeen, G.Y. Jeng, R.G. Kellogg, J. Kunkle, A.C. Mignerey, S. Nabili, F. Ricci-Tam, Y.H. Shin, A. Skuja, S.C. Tonwar, K. Wong

Massachusetts Institute of Technology, Cambridge, USA

D. Abercrombie, B. Allen, V. Azzolini, A. Baty, G. Bauer, R. Bi, S. Brandt, W. Busza, I.A. Cali, M. D'Alfonso, Z. Demiragli, G. Gomez Ceballos, M. Goncharov, P. Harris, D. Hsu, M. Hu, Y. Iiyama, G.M. Innocenti, M. Klute, D. Kovalskyi, Y.-J. Lee, P.D. Luckey, B. Maier, A.C. Marini, C. Mcginn, C. Mironov, S. Narayanan, X. Niu, C. Paus, C. Roland, G. Roland, G.S.F. Stephans, K. Sumorok, K. Tatar, D. Velicanu, J. Wang, T.W. Wang, B. Wyslouch, S. Zhaozhong

University of Minnesota, Minneapolis, USA

A.C. Benvenuti[†], R.M. Chatterjee, A. Evans, P. Hansen, J. Hiltbrand, Sh. Jain, S. Kalafut, Y. Kubota, Z. Lesko, J. Mans, N. Ruckstuhl, R. Rusack, M.A. Wadud

University of Mississippi, Oxford, USA

J.G. Acosta, S. Oliveros

University of Nebraska-Lincoln, Lincoln, USA

E. Avdeeva, K. Bloom, D.R. Claes, C. Fangmeier, F. Golf, R. Gonzalez Suarez, R. Kamalieddin, I. Kravchenko, J. Monroy, J.E. Siado, G.R. Snow, B. Stieger

State University of New York at Buffalo, Buffalo, USA

A. Godshalk, C. Harrington, I. Iashvili, A. Kharchilava, C. Mclean, D. Nguyen, A. Parker, S. Rappoccio, B. Roozbahani

Northeastern University, Boston, USA

G. Alverson, E. Barberis, C. Freer, A. Hortiangtham, D.M. Morse, T. Orimoto, R. Teixeira De Lima, T. Wamorkar, B. Wang, A. Wisecarver, D. Wood

Northwestern University, Evanston, USA

S. Bhattacharya, O. Charaf, K.A. Hahn, N. Mucia, N. Odell, M.H. Schmitt, K. Sung, M. Trovato, M. Velasco

University of Notre Dame, Notre Dame, USA

R. Bucci, N. Dev, M. Hildreth, K. Hurtado Anampa, C. Jessop, D.J. Karmgard, N. Kellams, K. Lannon, W. Li, N. Loukas, N. Marinelli, F. Meng, C. Mueller, Y. Musienko³⁵, M. Planer, A. Reinsvold, R. Ruchti, P. Siddireddy, G. Smith, S. Taroni, M. Wayne, A. Wightman, M. Wolf, A. Woodard

The Ohio State University, Columbus, USA

J. Alimena, L. Antonelli, B. Bylsma, L.S. Durkin, S. Flowers, B. Francis, A. Hart, C. Hill, W. Ji, T.Y. Ling, W. Luo, B.L. Winer

Princeton University, Princeton, USA

S. Cooperstein, P. Elmer, J. Hardenbrook, S. Higginbotham, A. Kalogeropoulos, D. Lange, M.T. Luchini, J. Luo, D. Marlow, K. Mei, I. Ojalvo, J. Olsen, C. Palmer, P. Piroué, J. Salfeld-Nebgen, D. Stickland, C. Tully

University of Puerto Rico, Mayaguez, USA

S. Malik, S. Norberg

Purdue University, West Lafayette, USA

A. Barker, V.E. Barnes, S. Das, L. Gutay, M. Jones, A.W. Jung, A. Khatiwada, B. Mahakud, D.H. Miller, N. Neumeister, C.C. Peng, S. Piperov, H. Qiu, J.F. Schulte, J. Sun, F. Wang, R. Xiao, W. Xie

Purdue University Northwest, Hammond, USA

T. Cheng, J. Dolen, N. Parashar

Rice University, Houston, USA

Z. Chen, K.M. Ecklund, S. Freed, F.J.M. Geurts, M. Kilpatrick, W. Li, B.P. Padley, R. Redjimi, J. Roberts, J. Rorie, W. Shi, Z. Tu, J. Zabel, A. Zhang

University of Rochester, Rochester, USA

A. Bodek, P. de Barbaro, R. Demina, Y.t. Duh, J.L. Dulemba, C. Fallon, T. Ferbel, M. Galanti, A. Garcia-Bellido, J. Han, O. Hindrichs, A. Khukhunaishvili, P. Tan, R. Taus

Rutgers, The State University of New Jersey, Piscataway, USA

A. Agapitos, J.P. Chou, Y. Gershtein, E. Halkiadakis, M. Heindl, E. Hughes, S. Kaplan, R. Kunnawalkam Elayavalli, S. Kyriacou, A. Lath, R. Montalvo, K. Nash, M. Osherson, H. Saka, S. Salur, S. Schnetzer, D. Sheffield, S. Somalwar, R. Stone, S. Thomas, P. Thomassen, M. Walker

University of Tennessee, Knoxville, USA

A.G. Delannoy, J. Heideman, G. Riley, S. Spanier

Texas A&M University, College Station, USA

O. Bouhali⁷³, A. Celik, M. Dalchenko, M. De Mattia, A. Delgado, S. Dildick, R. Eusebi, J. Gilmore, T. Huang, T. Kamon⁷⁴, S. Luo, R. Mueller, D. Overton, L. Perniè, D. Rathjens, A. Safonov

Texas Tech University, Lubbock, USA

N. Akchurin, J. Damgov, F. De Guio, P.R. Duderov, S. Kunori, K. Lamichhane, S.W. Lee, T. Mengke, S. Muthumuni, T. Peltola, S. Undleeb, I. Volobouev, Z. Wang

Vanderbilt University, Nashville, USA

S. Greene, A. Gurrola, R. Janjam, W. Johns, C. Maguire, A. Melo, H. Ni, K. Padeken, J.D. Ruiz Alvarez, P. Sheldon, S. Tuo, J. Velkovska, M. Verweij, Q. Xu

University of Virginia, Charlottesville, USA

M.W. Arenton, P. Barria, B. Cox, R. Hirosky, M. Joyce, A. Ledovskoy, H. Li, C. Neu, T. Sinthuprasith, Y. Wang, E. Wolfe, F. Xia

Wayne State University, Detroit, USA

R. Harr, P.E. Karchin, N. Poudyal, J. Sturdy, P. Thapa, S. Zaleski

University of Wisconsin - Madison, Madison, WI, USA

M. Brodski, J. Buchanan, C. Caillol, D. Carlsmith, S. Dasu, L. Dodd, B. Gomber, M. Grothe, M. Herndon, A. Hervé, U. Hussain, P. Klabbers, A. Lanaro, K. Long, R. Loveless, T. Ruggles, A. Savin, V. Sharma, N. Smith, W.H. Smith, N. Woods

†: Deceased

1: Also at Vienna University of Technology, Vienna, Austria

2: Also at IRFU, CEA, Université Paris-Saclay, Gif-sur-Yvette, France

3: Also at Universidade Estadual de Campinas, Campinas, Brazil

4: Also at Federal University of Rio Grande do Sul, Porto Alegre, Brazil

5: Also at Université Libre de Bruxelles, Bruxelles, Belgium

6: Also at University of Chinese Academy of Sciences, Beijing, China

7: Also at Institute for Theoretical and Experimental Physics, Moscow, Russia

8: Also at Joint Institute for Nuclear Research, Dubna, Russia

9: Now at Helwan University, Cairo, Egypt

10: Also at Zewail City of Science and Technology, Zewail, Egypt

11: Also at British University in Egypt, Cairo, Egypt

12: Now at Ain Shams University, Cairo, Egypt

13: Also at Department of Physics, King Abdulaziz University, Jeddah, Saudi Arabia

14: Also at Université de Haute Alsace, Mulhouse, France

15: Also at Skobeltsyn Institute of Nuclear Physics, Lomonosov Moscow State University, Moscow, Russia

16: Also at CERN, European Organization for Nuclear Research, Geneva, Switzerland

17: Also at RWTH Aachen University, III. Physikalisches Institut A, Aachen, Germany

18: Also at University of Hamburg, Hamburg, Germany

- 19: Also at Brandenburg University of Technology, Cottbus, Germany
- 20: Also at MTA-ELTE Lendület CMS Particle and Nuclear Physics Group, Eötvös Loránd University, Budapest, Hungary
- 21: Also at Institute of Nuclear Research ATOMKI, Debrecen, Hungary
- 22: Also at Institute of Physics, University of Debrecen, Debrecen, Hungary
- 23: Also at Indian Institute of Technology Bhubaneswar, Bhubaneswar, India
- 24: Also at Institute of Physics, Bhubaneswar, India
- 25: Also at Shoolini University, Solan, India
- 26: Also at University of Visva-Bharati, Santiniketan, India
- 27: Also at Isfahan University of Technology, Isfahan, Iran
- 28: Also at Plasma Physics Research Center, Science and Research Branch, Islamic Azad University, Tehran, Iran
- 29: Also at Università degli Studi di Siena, Siena, Italy
- 30: Also at Kyunghee University, Seoul, Korea
- 31: Also at International Islamic University of Malaysia, Kuala Lumpur, Malaysia
- 32: Also at Malaysian Nuclear Agency, MOSTI, Kajang, Malaysia
- 33: Also at Consejo Nacional de Ciencia y Tecnología, Mexico city, Mexico
- 34: Also at Warsaw University of Technology, Institute of Electronic Systems, Warsaw, Poland
- 35: Also at Institute for Nuclear Research, Moscow, Russia
- 36: Now at National Research Nuclear University 'Moscow Engineering Physics Institute' (MEPhI), Moscow, Russia
- 37: Also at St. Petersburg State Polytechnical University, St. Petersburg, Russia
- 38: Also at University of Florida, Gainesville, USA
- 39: Also at P.N. Lebedev Physical Institute, Moscow, Russia
- 40: Also at California Institute of Technology, Pasadena, USA
- 41: Also at Budker Institute of Nuclear Physics, Novosibirsk, Russia
- 42: Also at Faculty of Physics, University of Belgrade, Belgrade, Serbia
- 43: Also at INFN Sezione di Pavia ^a, Università di Pavia ^b, Pavia, Italy
- 44: Also at University of Belgrade, Faculty of Physics and Vinca Institute of Nuclear Sciences, Belgrade, Serbia
- 45: Also at Scuola Normale e Sezione dell'INFN, Pisa, Italy
- 46: Also at National and Kapodistrian University of Athens, Athens, Greece
- 47: Also at Riga Technical University, Riga, Latvia
- 48: Also at Universität Zürich, Zurich, Switzerland
- 49: Also at Stefan Meyer Institute for Subatomic Physics (SMI), Vienna, Austria
- 50: Also at Istanbul Aydin University, Istanbul, Turkey
- 51: Also at Mersin University, Mersin, Turkey
- 52: Also at Piri Reis University, Istanbul, Turkey
- 53: Also at Adiyaman University, Adiyaman, Turkey
- 54: Also at Gaziosmanpasa University, Tokat, Turkey
- 55: Also at Ozyegin University, Istanbul, Turkey
- 56: Also at Izmir Institute of Technology, Izmir, Turkey
- 57: Also at Marmara University, Istanbul, Turkey
- 58: Also at Kafkas University, Kars, Turkey
- 59: Also at Istanbul University, Faculty of Science, Istanbul, Turkey
- 60: Also at Istanbul Bilgi University, Istanbul, Turkey
- 61: Also at Hacettepe University, Ankara, Turkey
- 62: Also at Rutherford Appleton Laboratory, Didcot, United Kingdom
- 63: Also at School of Physics and Astronomy, University of Southampton, Southampton,

United Kingdom

64: Also at Monash University, Faculty of Science, Clayton, Australia

65: Also at Bethel University, St. Paul, USA

66: Also at Karamanoğlu Mehmetbey University, Karaman, Turkey

67: Also at Utah Valley University, Orem, USA

68: Also at Purdue University, West Lafayette, USA

69: Also at Beykent University, Istanbul, Turkey

70: Also at Bingol University, Bingol, Turkey

71: Also at Sinop University, Sinop, Turkey

72: Also at Mimar Sinan University, Istanbul, Istanbul, Turkey

73: Also at Texas A&M University at Qatar, Doha, Qatar

74: Also at Kyungpook National University, Daegu, Korea